J. Fluid Mech. (1994), *vol.* 278, *pp.* 1–31

The evolution equation for the flame surface density in turbulent premixed combustion

By ARNAUD TROUVÉ[1]† AND THIERRY POINSOT[2]

[1] Center for Turbulence Research, Stanford University, Stanford, CA 94305, USA

[2] CNRS, Institut de Mécanique des Fluides de Toulouse, 31400, France

(Received 15 March 1993 and in revised form 25 March 1994)

One basic effect of turbulence in turbulent premixed combustion is for the fluctuating velocity field to wrinkle the flame and greatly increase its surface area. In the flamelet theory, this effect is described by the flame surface density. An exact evolution equation for the flame surface density, called the Σ-equation, may be written, where basic physical mechanisms like production by hydrodynamic straining and destruction by propagation effects are described explicitly. Direct numerical simulation (DNS) is used in this paper to estimate the different terms appearing in the Σ-equation. The numerical configuration corresponds to three-dimensional premixed flames in isotropic turbulent flow. The simulations are performed for various mixture Lewis numbers in order to modify the strength and nature of the flame–flow coupling. The DNS-based analysis provides much information relevant to flamelet models. In particular, the flame surface density, and the source and sink terms for the flame surface density, are resolved spatially across the turbulent flame brush. The geometry as well as the dynamics of the flame differ quite significantly from one end of the reaction zone to the other. For instance, contrary to the intuitive idea that flame propagation effects merely counteract the wrinkling due to the turbulence, the role of flame propagation is not constant across the turbulent brush and switches from flame surface production at the front to flame surface dissipation at the back. Direct comparisons with flamelet models are also performed. The Bray–Moss–Libby assumption that the flame surface density is proportional to the flamelet crossing frequency, a quantity that can be measured in experiments, is found to be valid. Major uncertainties remain, however, over an appropriate description of the flamelet crossing frequency. In comparison, the coherent flame model of Marble & Broadwell achieves closure at the level of the Σ-equation and provides a more promising physically based description of the flame surface dynamics. Some areas where the model needs improvement are identified.

1. Introduction

Flamelet models constitute one of the most common approaches for turbulent premixed combustion (Bray 1980; Williams 1985; Peters 1986; Poinsot, Veynante & Candel 1991). Such models are very attractive, as they conveniently separate the combustion problem from the analysis of the turbulent flow field. These models are based on the 'flame sheet' assumption, which requires chemical reaction to occur at fast timescales and short lengthscales relative to the turbulence. In this situation, the flame is confined to relatively thin layers within the turbulent flow field and the reaction zone is a burning surface.

† Present address: Institut Français du Pétrole, 1 et 4, avenue de Bois-Préau, BP 311, 92506 Rueil-Malmaison, France.

Experimental evidence suggests that the topology of the reaction zone can indeed often be described as a continuous burning surface, and many practical premixed flame configurations are therefore believed to occur in the flamelet regime. Clearly, however, the flamelet regime is not the only possible premixed combustion mode and it is important to determine the domain of validity of the 'flame sheet' assumption. Unfortunately, the boundaries of this domain are not known with precision. In fact, different theories leading to significantly different predictions can be found in the literature (Williams 1985; Poinsot *et al.* 1991; Roberts *et al.* 1993). We refer the reader to the discussion of figure 1 in §3.1 for further details on this matter and consider in the meantime a combustion problem with sufficiently fast reaction.

In the flamelet regime, it is convenient to describe the flame–flow interactions in terms of the following two basic ingredients: a speed that characterizes the flame inner structure, and a surface area that characterizes the flame wrinkling. Within the flamelet formulation, these two ingredients appear both in the descriptions of local (spatially resolved) and global (space-averaged) flame properties.

For instance, the local mean reaction rate may be written as a mean integrated chemical rate times the flame surface density:

$$\langle \dot{\omega}_R \rangle = \left\langle \int \dot{\omega}_R \, \mathrm{d}n \right\rangle_S \langle \Sigma' \rangle = \left\langle \int \dot{\omega}_R \, \mathrm{d}n \right\rangle_S \Sigma, \tag{1}$$

where $\dot{\omega}_R$ is the mass of fuel consumed per unit time and per unit volume; $\int \dot{\omega}_R \, \mathrm{d}n$ is the local integral of the reaction rate along the flame normal direction; Σ' is the flame surface area per unit volume; Σ is the flame surface density, defined as the expected value for Σ', $\Sigma \equiv \langle \Sigma' \rangle$. Note that in (1), all quantities are local and mean operators correspond to ensemble-averaging. While $\langle\ \rangle$ denotes a standard, unweighted ensemble-average, $\langle\ \rangle_S$ denotes a surface mean, defined as an area-weighted ensemble-average (Pope 1988), $\langle Q \rangle_S \equiv \langle Q\Sigma' \rangle / \langle \Sigma' \rangle = \langle Q\Sigma' \rangle / \Sigma$.

In (1), the integral of the reaction rate can be replaced by the local fuel consumption speed, S_C, defined as

$$S_C \equiv \frac{1}{\rho_u Y_{R,u}} \int \dot{\omega}_R \, \mathrm{d}n, \tag{2}$$

where ρ_u and $Y_{R,u}$ are respectively the density and the fuel mass fraction in the unburnt gas. S_C characterizes the local combustion intensity. The mean reaction rate may then be expressed as the surface mean of S_C, called the flamelet speed, times the flame surface density:

$$\langle \dot{\omega}_R \rangle = (\rho_u Y_{R,u} \langle S_C \rangle_S) \Sigma. \tag{3}$$

Equation (3) is the classical flamelet expression for the ensemble mean of the reaction rate. In general, this mean reaction rate is a function of both position and time, $\langle \dot{\omega}_R \rangle (x, t)$. An overall reaction rate can also be obtained by space-averaging (3) over an arbitrary volume, V, that encloses the reaction zone:

$$\overline{\langle \dot{\omega}_R \rangle}(t) \equiv \frac{1}{V} \int \langle \dot{\omega}_R \rangle (x, t) \, \mathrm{d}V = (\rho_u Y_{R,u} \widehat{S_C}(t)) \bar{\Sigma}(t), \tag{4}$$

where $\widehat{S_C}(t)$ and $\bar{\Sigma}(t)$ are defined by the following expressions:

$$\widehat{S_C}(t) \equiv \left(\int \langle S_C \rangle_S (x, t) \, \Sigma(x, t) \, \mathrm{d}V \right) \Big/ \left(\int \Sigma(x, t) \, \mathrm{d}V \right), \tag{5}$$

$$\bar{\Sigma}(t) \equiv \frac{1}{V} \int \Sigma(x, t) \, \mathrm{d}V = \frac{\langle S_V \rangle (t)}{V}, \tag{6}$$

where $S_V(t)$ is the total flame surface area within V at time t. By definition, $\langle S_V \rangle$ is equal to the volume integral of the flame surface density.

$\widehat{S_C}$ and $\langle S_V \rangle$ are global flame properties. Using (4) and (6), they are simply related to the turbulent flame speed, S_T:

$$S_T(t) \equiv \frac{1}{\rho_u Y_{R,u} S_p} \int \langle \dot{\omega}_R \rangle (x, t) \, \mathrm{d}V = \widehat{S_C}(t) \frac{\langle S_V \rangle (t)}{S_p}, \tag{7}$$

where S_p is the projected area of the flame on a surface perpendicular to the direction of mean propagation.

The flamelet speed, $\langle S_C \rangle_S$, in (3) and the mean fuel consumption speed, $\widehat{S_C}$, in (4) and (7) account for local variations of the reaction rate along the flame surface. Laminar flame theory indicates that the local flame structure is modified by flow divergence, usually characterized by the strain rate acting in the flame tangent plane, as well as by flame front curvature (Clavin 1985; Williams 1985; Law 1988). The magnitude of these variations depends strongly on the molecular diffusive properties of the burning mixture. For an inert-abundant, fuel-lean or fuel-rich mixture, this effect can be analysed in terms of an effective Lewis number, defined as the ratio of thermal diffusivity to the mass diffusivity of the deficient reactant. When heat and the deficient reactant diffuse identically, i.e. when the Lewis number is unity, the structure of adiabatic unrestrained flames shows little alteration and remains approximately uniform along the reactive sheets. For non-unity Lewis numbers, however, differential diffusion of heat and species results in a strong sensitivity of the flame structure to strain rate and curvature.

Furthermore, besides being affected by differential diffusion, the flame response is also strongly affected by the presence of heat loss (Libby & Williams 1983). Under certain conditions, the variations in flame intensity can become critical and lead to partial or total quenching of the flame. Recent numerical studies (Poinsot *et al.* 1991), however, as well as experimental results (Roberts *et al.* 1993), suggest that quenching is a rather unlikely event for turbulent premixed combustion (we are referring here to combustion problems without walls). In addition, although the local combustion intensity may exhibit large fluctuations along the turbulent flame front, particularly for non-unity Lewis number flames, and although these fluctuations may in turn result in strong spatial variations of the flamelet speed, $\langle S_C \rangle_S$, across the turbulent flame brush, direct simulations suggest that these departures from the laminar consumption rate have the remarkable tendency to cancel in the mean, i.e. when averaged over the whole flame (Ashurst, Peters & Smooke 1987; Haworth & Poinsot 1992; Rutland & Trouvé 1993). In previous numerical studies, where the Lewis number takes values between 0.8 and 1.2, the mean fuel consumption speed, $\widehat{S_C}$, was determined to remain within 10% to 30% of the one-dimensional laminar flame speed value, s_L.

Thus, for flames with Lewis numbers close to unity, it appears that the mean fuel consumption speed, $\widehat{S_C}$, is only weakly sensitive to the flow field and the principal effect of turbulence is for the fluctuating velocity field to wrinkle the flame and greatly increase its surface area. This phenomenon is represented in (3) by the flame surface density, Σ.

In flamelet models, the flame surface density is obtained either using an algebraic closure, like in current formulations of the Bray–Moss–Libby model (Bray, Libby & Moss 1984; Bray, Champion & Libby 1989; Bray 1990), or via a modelled transport equation, called the Σ-equation (Marble & Broadwell 1977; Darabiha *et al.* 1987; Pope & Cheng 1988; Maistret *et al.* 1989; Candel *et al.* 1990; Cant, Pope & Bray 1990; Borghi 1990; Mantel & Borghi 1994). The Σ-equation was first postulated by Marble

& Broadwell (1977) on phenomenological grounds. Recent theoretical work has produced a more rigorous approach that leads to an exact, but unclosed, formulation for the turbulent Σ-equation (Pope 1988; Candel & Poinsot 1990). Unfortunately, the flame surface density and the different terms of interest in the turbulent Σ-equation are not experimentally accessible. Comparisons between model predictions and experimental results are usually performed with limited data sets and for global quantities like the turbulent flame speed (Duclos, Veynante & Poinsot 1993). These comparisons do not allow a direct critical evaluation of the closure assumptions used in current flamelet models and, as a result, the domain of validity of these assumptions is unknown.

The objective of this research is to provide methods for sensitive testing of modelling ideas used in turbulent combustion. In the following, direct numerical simulation (DNS) is used to get basic information on the dynamics of flame surface densities. The paper is organized as follows. The theoretical framework for analysis of the flame surface density and the formulation of its exact transport equation are first reviewed in §2. Direct simulations of turbulent premixed flames are then used in the remainder of the paper to estimate the different terms appearing in the turbulent Σ-equation. The numerical methods and numerical configuration are presented in §3.1. A new methodology to extract the flame surface density and other relevant quantities from the DNS database is described in §3.2. Results obtained with this new methodology are presented in §4. These include descriptions of global properties (§4.1) as well as local properties (§4.2) of turbulent flames with different Lewis numbers. In §4.2, the Σ-profiles, and the source and sink terms for Σ that determine production or dissipation of flame surface area are resolved spatially throughout the turbulent flame brush. Finally, detailed comparisons with flamelet models are performed and some shortcomings in current formulations are discussed in §5.

2. Theory

An empirical transport equation for the flame surface density was first postulated by Marble & Broadwell (1977). Using conservation equations for elementary volumes and surfaces embedded in a turbulent flow field, a more rigorous approach was later proposed by Pope (1988) and Candel & Poinsot (1990) who derive an exact balance equation for the flame surface-to-volume ratio, Σ':

$$\frac{\partial \Sigma'}{\partial t} + \nabla \cdot \dot{\boldsymbol{X}} \Sigma' = (\nabla \cdot \dot{\boldsymbol{X}} - \boldsymbol{nn} : \nabla \dot{\boldsymbol{X}}) \Sigma', \tag{8}$$

where $\dot{\boldsymbol{X}}$ is the velocity of the flame surface, given by the sum of the fluid velocity and the flame propagation speed in the normal direction: $\dot{\boldsymbol{X}} = \boldsymbol{u} + w\boldsymbol{n}$; $\boldsymbol{n}$ is the unit vector normal to the flame surface; and where we use standard tensorial notation: $(\boldsymbol{nn} : \nabla \dot{\boldsymbol{X}}) = n_i n_j \partial \dot{X}_i / \partial x_j$.

The right-hand side of (8) can also be expressed in terms of flame stretch. The flame stretch, κ, is defined as the rate of change of a Lagrangian flame surface element, δA:

$$\kappa = \frac{1}{\delta A} \frac{\mathrm{d}(\delta A)}{\mathrm{d}t} = \frac{1}{\delta A} \left\{ \frac{\partial (\delta A)}{\partial t} + \dot{\boldsymbol{X}} \cdot \nabla (\delta A) \right\}. \tag{9}$$

A more useful expression for κ is in terms of strain rate, flame curvature and flame propagation speed (see for example Candel & Poinsot 1990):

$$\kappa = a_T + 2wk_m, \tag{10}$$

where a_T is the rate of strain acting in the flame tangent plane: $a_T = \nabla \cdot \boldsymbol{u} - \boldsymbol{nn}: \nabla \boldsymbol{u}$; and k_m is the flame surface curvature, as given by the divergence of the flame normal direction: $2k_m = \nabla \cdot \boldsymbol{n}$. In (10), positive curvature is chosen convex towards the reactants.

Using (10), the balance equation for the flame surface-to-volume ratio can be re-written as

$$\frac{\partial \Sigma'}{\partial t} + \nabla \cdot \dot{\boldsymbol{X}} \Sigma' = \kappa \Sigma'. \tag{11}$$

When ensemble-averaged, this equation yields an exact balance equation for the flame surface density, Σ (Pope 1988; Cant *et al.* 1990):

$$\frac{\partial \Sigma}{\partial t} + \nabla \cdot \langle \dot{\boldsymbol{X}} \rangle_S \Sigma = \langle \kappa \rangle_S \Sigma. \tag{12}$$

Note that, as mentioned in the introduction, surface means are different from standard means. Also, the surface mean of a quantity Q should not be confused with the ensemble mean of Q conditioned on being at the flame location: the former is a weighted average, the latter is not (see §3.2).

Equation (12) can be cast in various forms. For modelling purposes, it is useful to split the velocity vector into a mean component and a turbulent fluctuation: $\boldsymbol{u} = \tilde{\boldsymbol{U}} + \boldsymbol{u}''$, where the tilde denotes a Favre-averaged quantity: $\tilde{\boldsymbol{U}} = \langle \rho \boldsymbol{U} \rangle / \langle \rho \rangle$. We can then re-write (12) as follows:

$$\frac{\partial \Sigma}{\partial t} + \nabla \cdot \tilde{\boldsymbol{U}} \Sigma + \nabla \cdot \langle \boldsymbol{u}'' \rangle_S \Sigma + \nabla \cdot \langle w \boldsymbol{n} \rangle_S \Sigma = \langle a_T \rangle_S \Sigma + \langle A_T \rangle_S \Sigma + 2 \langle w k_m \rangle_S \Sigma, \tag{13}$$

where we use the following notation:

$$\langle a_T \rangle_S = \langle \nabla \cdot \boldsymbol{u}'' - \boldsymbol{nn}: \nabla \boldsymbol{u}'' \rangle_S, \tag{14}$$

$$\langle A_T \rangle_S = \nabla \cdot \tilde{\boldsymbol{U}} - \langle \boldsymbol{nn} \rangle_S: \nabla \tilde{\boldsymbol{U}}. \tag{15}$$

The three convective terms on the left-hand side of (13) are transport terms that correspond respectively to convection by the mean flow, turbulent diffusion and flame propagation. The terms on the right-hand side of the equation are the source and sink terms for the flame surface density: $\langle a_T \rangle_S$ is the turbulent strain rate acting in the flame tangent plane, $\langle A_T \rangle_S$ is the strain rate due to the mean flow field, and $2\langle w k_m \rangle_S$ is a term that accounts for the combined effects of flame curvature and flame propagation.

Equation (13) is an exact expression of the evolution equation for the flame surface density in a turbulent flow field. Unfortunately, many terms remain unclosed in this exact turbulent Σ-equation. Modelling assumptions are therefore required, in particular to calculate the turbulent diffusion term and the turbulent flame stretch. Our concern in this study is the validation of these modelling assumptions.

Although much progress has been reported in recent years in the development of experimental techniques that monitor the flame position (for instance spontaneous light emission measurements, laser tomography and laser induced fluorescence) and techniques that resolve the velocity gradients (in particular particle tracking velocimetry and particle image velocimetry), measuring a flame-based quantity like stretch in a turbulent flow environment remains a very difficult task. While strain rate measurements have been reported in studies of laminar flame–vortex interaction (Driscoll *et al.* 1993), such measurements have not yet been attempted in turbulent flames. Thus, experiments provide little guidance for modelling the turbulent Σ-

equation. In this context, a numerical approach is a particularly attractive alternative. In the following, we describe three-dimensional DNS of premixed flames embedded in isotropic turbulence.

3. Direct numerical simulation of turbulent premixed flames

3.1. *Numerical methods and numerical configuration*

We use DNS to analyse the different terms in the equation for the flame surface density. The simulations are performed using a three-dimensional compressible Navier–Stokes solver that fully resolves the turbulent flow field. The solver uses a high-order finite-difference scheme: spatial derivatives are computed with a modified Padé scheme that is sixth-order accurate (Lele 1992); solutions are advanced in time with a third-order Runge–Kutta method (Wray 1990); boundary conditions are specified with the NSCBC method (Poinsot & Lele 1992). We refer the reader to Lele (1992) and Poinsot & Lele (1992) for further details concerning the system of equations solved and the numerical methods.

Because of the otherwise prohibitive computational cost, simulations are limited to simple but finite-rate reaction schemes. In this work, the chemistry model is a single-step irreversible chemical reaction where the reaction rate depends exponentially on temperature (Arrhenius kinetics):

$$\dot{\omega}_R = B\rho\, Y_R \exp(-T_a/T), \tag{16}$$

where T_a is the activation temperature and B is a constant that is determined according to the selected laminar flame speed. This formulation corresponds to a binary reaction in which one of the reactants, Y_R, is strongly deficient; for example, in fuel-lean combustion. Also, it is worth emphasizing that the simulations do not use the constant-density assumption, the reaction is exothermic and heat release effects are fully accounted for.

Following Williams (1985), we re-write the reaction rate as

$$\dot{\omega}_R = A\rho\, Y_R \exp\left(\frac{-\beta(1-\Theta)}{1-\alpha(1-\Theta)}\right), \tag{17}$$

where Θ is the reduced temperature, $\Theta = (T-T_u)/(T_b-T_u)$; T_u is the temperature of the fresh reactants; T_b is the adiabatic flame temperature; and the coefficients A, α, and β are, respectively, the reduced pre-exponential factor, the heat release factor, and the reduced activation energy:

$$A = B\exp(-\beta/\alpha), \quad \alpha = (T_b-T_u)/T_b, \quad \beta = \alpha T_a/T_b. \tag{18}$$

Values of the flame parameters are reported in table 1. A has dimensions of T^{-1} and is specified so that the laminar flame speed, s_L, remains constant throughout all simulated cases.

Another important feature of the simulations is that the transport coefficients are temperature dependent. These coefficients satisfy the following relations:

$$\mu = \mu_u(T/T_u)^b, \quad Le = \lambda_{th}/\rho D c_p = \text{constant}, \quad Pr = \mu c_p/\lambda_{th} = \text{constant}, \tag{19}$$

where μ, λ_{th} and D are the molecular diffusivities of, respectively, momentum, internal energy and species mass; c_p is the specific heat at constant pressure; b is a constant; and Le and Pr are respectively the Lewis number and the Prandtl number. Simulations have been performed for four different Lewis numbers, $Le = 0.3$, 0.8, 1.0, and 1.2 (table

Le	α	β	A^+	b	Pr
0.3	0.75	8.0	972	0.76	0.75
0.8	0.75	8.0	456	0.76	0.75
1.0	0.75	8.0	386	0.76	0.75
1.2	0.75	8.0	332	0.76	0.75

TABLE 1. Dimensionless flame parameters for the four simulated cases. A is made non-dimensional by the laminar flame time, $A^+ = A(\lambda_{th}/\rho c_p)_u/s_L^2$

t/τ_0	u'/s_L	l/l_F	v_k/s_L	η_k/l_F	Re_l	Re_λ	Da
0	10.0	5.2	2.8	0.27	70.0	50.0	0.37
2.5	4.9	5.2	2.3	0.32	33.5	17.5	0.54
4.3	3.3	5.6	1.7	0.43	24.3	13.5	0.98

TABLE 2. Dimensionless parameters for the simulations. The first row is the initial condition ($t = 0$); the second row is at normalized time $t/\tau_0 \approx 2.5$, and the third row is at time $t/\tau_0 \approx 4.3$, where τ_0 is the initial turbulent eddy turnover time

1). The Lewis number is modified by changing the value of the mass diffusivity in the unburnt gas, D_u. The laminar flame thickness, defined as $l_F = (\lambda_{th}/\rho c_p)_u/s_L$, remains constant throughout all simulated cases.

The computational configuration corresponds to a premixed flame embedded in a three-dimensional decaying isotropic turbulent flow. The calculations are initialized with fresh reactants on the left-hand side of the domain ($x < 0$) and burnt products on the right ($x > 0$); the two are separated by a plane laminar flame. Isotropic turbulence is initially located in the flow of fresh reactants, its velocity field being specified according to a model energy spectrum:

$$E(k) = C(k/k_t)^4 \exp\{-2(k/k_t)^2\}, \tag{20}$$

where k is the wavenumber; and C and k_t are model parameters that are specified according to, respectively, the initial turbulent r.m.s. velocity, u', and integral lengthscale, l. The left- and right-hand sides of the computational domain are inflow and outflow boundaries, while periodic boundary conditions are applied at lateral walls. Non-periodic boundary conditions are needed along x due to the density change from unburnt to burnt gases. Note, however, that no turbulence is generated at the inflow boundary and the simulations are time-evolving rather than space-evolving.

Values of the run parameters are reported in table 2. At time $t = 0$, the turbulence is characterized by a Kolmogorov lengthscale smaller than the laminar flame thickness, $\eta_k/l_F < 1$, and a turbulence intensity that is much higher than the laminar flame speed, $u'/s_L = 10$. The initial turbulent Reynolds number based on the Taylor microscale, λ, is $Re_\lambda = 50$. The initial turbulent Reynolds number based on the integral lengthscale is $Re_l = 70$. In table 2, a Damköhler number is also introduced using the Kolmogorov timescale and the laminar flame time: $Da = (\lambda/u')/(l_F/s_L) = \sqrt{15}(\eta_k/v_k)/(l_F/s_L)$, where v_k is the Kolmogorov velocity. The simulated flames correspond to relatively low Damköhler numbers, $Da < 1$. Also the grid spacing is uniform in all three directions. The resolution is 129^3, except for the $Le = 0.3$ case where a $129 \times 65 \times 65$ grid was used (129 mesh points in the direction of mean flame propagation, x).

Our choice of the run parameters has been dictated by the desire to simulate turbulent flows with the highest possible Reynolds numbers, while still resolving the

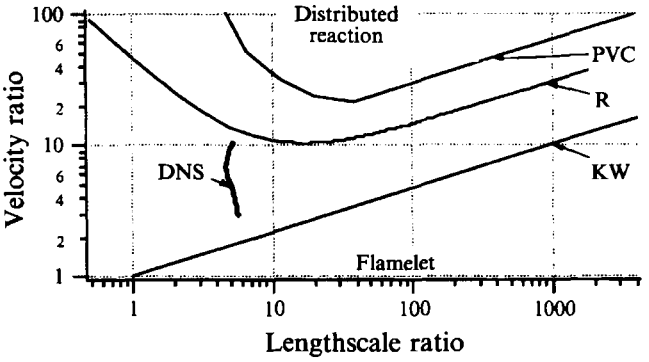

FIGURE 1. Time evolution of the DNS flame–flow conditions in a turbulent combustion diagram parametrized by $(l/l_F, u'/s_L)$, and where the boundary separating the flamelet regime and the distributed reaction regime is estimated according to: the Klimov–Williams criterion, (KW); the Poinsot *et al.* criterion (PVC); the Roberts *et al.* criterion (R). The simulations correspond to nonflamelet combustion according to KW and to flamelet combustion according to PVC and R.

flame structure as well as maintaining flame and flow conditions consistent with the flamelet picture. This last aspect is now discussed in more detail.

Following Poinsot *et al.* (1991), the domain of validity of the flamelet picture is considered in figure 1, in a turbulent combustion diagram whose coordinates are the relative flow to flame length and velocity scale ratios, l/l_F and u'/s_L. Equivalent plots but with different selections of coordinates are given in Bray (1980), Williams (1985), Peters (1986). Two important combustion regimes are identifiable in figure 1: the flamelet regime and the regime of distributed reaction. The former corresponds to fast flame-sheet reaction, and is the focus of the present study; the latter occurs when turbulent mixing is rapid enough compared to the chemistry, thereby causing the reaction zone to become volume filling. The precise location of the boundary separating these two limiting regimes remains an open question.

According to the classical Klimov–Williams criterion (KW), flamelet combustion occurs when the laminar flame time is shorter than the Kolmogorov time, $l_F/s_L < \eta_k/v_k$, or equivalently $(u'/s_L)^3 < l/l_F$ (see figure 1). While being a valuable first-order estimate, KW is based on dimensional analysis and its accuracy is uncertain. For instance, KW is derived from the assumption that the maximum turbulent flame stretch is produced by the Kolmogorov eddies, whereas two recent studies of laminar flame–vortex interactions, a numerical study by Poinsot *et al.* (1991) and an experimental study by Roberts *et al.* (1993), find that the smallest flow scales cannot influence the flame structure because they lack sufficient energy. Both studies argue that the KW criterion underestimates the size of the flamelet domain, and propose modified criteria (PVC and R, respectively) to predict flamelet combustion. As seen in figure 1, PVC and R differ significantly from KW, particularly at small lengthscale ratios, $l/l_F < 30$.

Since the present simulations feature decaying turbulence, the DNS characteristics are time evolving and are represented by a line segment in figure 1. This line segment is within the flamelet domain according to PVC and R, but outside that domain according to KW. In the absence of agreement among the above three criteria, a careful direct examination of the instantaneous flame topology was performed using three-dimensional graphics. Visual inspections of the flame topology are well-suited to determine whether the chemical reaction is flamelet-like and occurs in surfaces (characterized by a thickness close to the laminar flame thickness, l_F) or is distributed

and occurs in volumes (characterized by a size much larger than l_F). We found that despite the low flame Damköhler numbers, the reaction zone can still be described as a surface (see figure 6) and the simulated flames occur in the flamelet regime.

In summary, the simulated flames are believed to be representative of the flamelet regime. The simulations describe the wrinkling of the flame zone by turbulent motions as well as the effect of combustion on the flow due to dilatation and temperature-dependent transport properties. The Lewis number is used as a control parameter to modify the strength and the nature of the coupling between the chemistry and the turbulence.

3.2. *Diagnostics*

All terms in (13) can be obtained from the simulations. We now briefly describe how. The velocity vector and the velocity-gradient tensor are readily obtained from the resolved flow field. To define flame-based quantities, we make use of the thin-flame picture. First, a progress variable, c, is introduced to indicate location within the reaction zone, $c = 1-(Y_R/Y_{R,u})$. The progress variable varies monotonically through the flame from 0 in the reactants to 1 in the products. Constant-progress-variable surfaces may conveniently be used to define the flame front location. Note that this definition of the flame surface might appear questionable in the present simulations owing to the presence of small turbulent eddies in the preheat zone ($0 < c < 0.6$). These eddies, however, dissipate rapidly, before they can reach the reaction zone ($0.7 < c < 0.9$). Thus, in the reaction zone, the constant-c surfaces are approximately parallel and the choice of a particular c-contour to define the flame front location appears as a valid approximation: we use the surface $c = c_f = 0.8$. In addition, at any location on this surface the local gradient of c defines the normal direction to the flame front:

$$\boldsymbol{n} = -\nabla c/|\nabla c|, \tag{21}$$

where $\boldsymbol{n}$ points into the fresh reactants.

The propagation speed of the flame surface, w, is obtained from an expression analogous to the well-known field equation (also called the G-equation, see for example Kerstein, Ashurst & Williams 1988). Let us first consider a point on the flame surface, $c = c_f$. The velocity, $\dot{\boldsymbol{X}}$, at which this point must move to remain on the surface is given by

$$\frac{\partial c}{\partial t} + \dot{\boldsymbol{X}} \cdot \nabla c = 0, \tag{22}$$

which, using (21), implies that

$$\dot{\boldsymbol{X}} \cdot \boldsymbol{n} = \frac{1}{|\nabla c|}\frac{\partial c}{\partial t}, \tag{23}$$

and yields the following expression for the flame propagation speed:

$$w = \dot{\boldsymbol{X}} \cdot \boldsymbol{n} - \boldsymbol{u} \cdot \boldsymbol{n} = \frac{1}{|\nabla c|}\frac{\mathrm{D}c}{\mathrm{D}t}, \tag{24}$$

where the quantities are evaluated at the surface $c = c_f$. In the simulations we solve a conservation equation for the fuel mass fraction, Y_R, and since by definition $c = 1-(Y_R/Y_{R,u})$, the expression above can be readily obtained from the DNS database:

$$w = \frac{1}{\rho|\nabla Y_R|}(\dot{\omega}_R - \nabla \cdot (\rho D \nabla Y_R)). \tag{25}$$

The flame surface density, Σ, is a more subtle quantity. It includes both geometrical and statistical information. Following Pope (1990), the flame surface density is

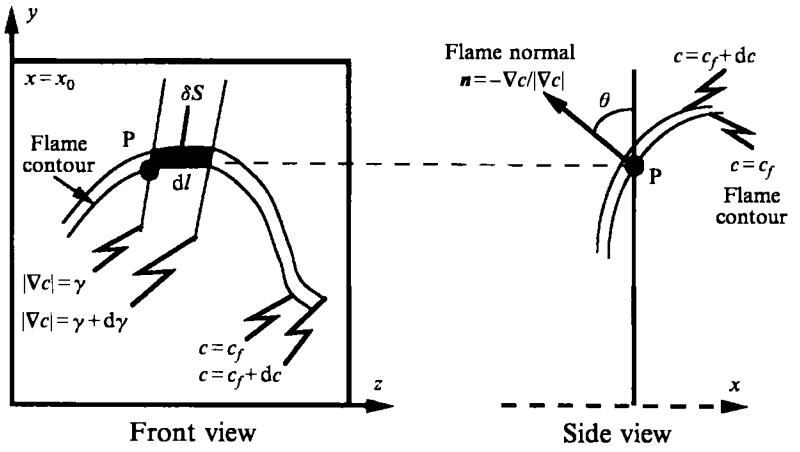

FIGURE 2. A geometrical expression for the joint probability of the progress variable and the magnitude of its gradient in a given (y, z)-plane: $p(c_f, \gamma)\,\mathrm{d}c\,\mathrm{d}\gamma = \textit{probability}(c_f \leqslant c \leqslant c_f + \mathrm{d}c; \gamma \leqslant |\nabla c| \leqslant \gamma + \mathrm{d}\gamma) = \delta S / L_y L_z$, and $\delta S = \mathrm{d}l(\mathrm{d}c/\gamma|\cos\theta|)$, see (29).

expressed as the product of the expected value for the magnitude of the gradient of c, conditioned on being on the flame surface, times the probability of being on that surface:

$$\Sigma' = |\nabla c|\,\delta(c - c_f), \quad \text{and} \quad \Sigma \equiv \langle \Sigma' \rangle = \langle |\nabla c| \,|\, c = c_f \rangle p(c_f), \tag{26}$$

where $p(c_f)$ is the probability of $c = c_f$. An equivalent expression for Σ, also proposed by Pope (1990), is in terms of the joint probability of the scalar c and the magnitude of its gradient:

$$\Sigma = \int_0^\infty \gamma p(c_f, \gamma)\,\mathrm{d}\gamma, \tag{27}$$

where $\gamma = |\nabla c|$.

We now turn to the averaging problem. In the simulations, the flame brush propagates along the x-direction, and the problem remains homogeneous in the (y, z)-planes. Therefore, averaged quantities depend on x and time t only, and ensemble-averaging can be performed in the (y, z)-planes:

$$\langle Q \rangle (x, t) = \frac{1}{L_y L_z} \int Q(x, y, z, t)\,\mathrm{d}y\,\mathrm{d}z, \tag{28}$$

where L_y and L_z are the y- and z-dimensions of the computational domain. Since the flow field is non-stationary, time-averaging cannot be used and the present analysis is based exclusively on slicing the DNS database in planes perpendicular to the direction of mean flame propagation.

Let us now consider a particular (y, z)-plane, $x = x_0$. In that plane, the flame contour $c = c_f$ is generically a set of closed lines. The flame surface density, as well as the various surface and conditional means in the analysis, can be expressed in terms of line integrals along this $(c = c_f, x = x_0)$ line contour. For instance, as suggested by (27), the flame surface density, Σ, can be obtained via the joint probability $p(c_f, \gamma)$. Simple geometrical considerations lead to the following relation (see figure 2):

$$p(c_f, \gamma)\,\mathrm{d}\gamma = \frac{1}{L_y L_z} \sum_{j=1}^{J} \frac{\mathrm{d}l}{\gamma |\cos\theta|}, \tag{29}$$

where $\mathrm{d}l$ designates the arclength of an infinitesimal flame element on the line contour $c = c_f$, and θ is a measure of the orientation of this flame element with respect to the $x = x_0$ plane. In (29), summation is over all occurrences of the event $(c, |\nabla c|) = (c_f, \gamma)$.

Combining (27) and (29), a convenient expression for Σ is obtained:

$$\Sigma = \frac{1}{L_y L_z}\int_{c=c_f}\frac{\mathrm{d}l}{|\cos\theta|} = \frac{1}{L_y L_z}\int_{c=c_f}\frac{|\nabla c|}{[(\partial c/\partial y)^2+(\partial c/\partial z)^2]^{1/2}}\,\mathrm{d}l, \tag{30}$$

where we use the geometrical relation: $|\cos\theta| = [(\partial c/\partial y)^2+(\partial c/\partial z)^2]^{1/2}/|\nabla c|$.

Also, integrating (29) over all possible values of γ gives an estimate for the probability $p(c_f)$:

$$p(c_f) = \int_0^\infty p(c_f,\gamma)\,\mathrm{d}\gamma = \frac{1}{L_y L_z}\int_{c=c_f}\frac{\mathrm{d}l}{|\cos\theta|\,|\nabla c|} = \frac{1}{L_y L_z}\int_{c=c_f}\frac{\mathrm{d}l}{[(\partial c/\partial y)^2+(\partial c/\partial z)^2]^{1/2}}, \tag{31}$$

which in turn can be used to derive the following expressions for conditional and surface means:

$$\langle Q\,|\,c=c_f\rangle = \frac{\langle Q\delta(c-c_f)\rangle}{p(c_f)} = \frac{\displaystyle\int_{c=c_f}(Q\,\mathrm{d}l/|\cos\theta|\,|\nabla c|)}{\displaystyle\int_{c=c_f}(\mathrm{d}l/|\cos\theta|\,|\nabla c|)}, \tag{32}$$

$$\langle Q\rangle_S \equiv \frac{\langle Q\Sigma'\rangle}{\langle\Sigma'\rangle} = \frac{\langle Q|\nabla c|\,|\,c=c_f\rangle}{\langle|\nabla c|\,|\,c=c_f\rangle} = \frac{\displaystyle\int_{c=c_f}(Q\,\mathrm{d}l/|\cos\theta|)}{\displaystyle\int_{c=c_f}(\mathrm{d}l/|\cos\theta|)}. \tag{33}$$

Clearly, surface means differ from standard means, $\langle Q\rangle_S \neq \langle Q\rangle$, as well as from conditional means, $\langle Q\rangle_S \neq \langle Q\,|\,c=c_f\rangle$.

The relations above provide a methodology to estimate the different means needed in our analysis. The accuracy of these expressions depends on the size of the computational domain with respect to the turbulent lengthscales. In the simulations, the integral lengthscale, l, of the turbulent flow field grows as the kinetic energy decays; this growth, however, is rather slow, and it has been determined that l remains at least 8 times smaller than L_y and L_z. In any case, we recognize that the statistics are somewhat undersampled. For instance, the DNS-based profiles presented in §4.2 are rough and sometimes spiky, which clearly suggests that statistical convergence is not fully achieved. These errors, however, are deemed acceptable as long as the basic features of the profiles are captured correctly.

4. Results and discussion

4.1. *Global flame properties*

The expressions (5), (6) and (7) in the introduction give the general relationship between the local mean quantities, $\langle S_C\rangle_S$ and Σ, and the more familiar global flame properties, $\widehat{S_C}$, $\langle S_V\rangle$ and S_T. Also, as described in the previous section, the analysis takes advantage of the fact that the simulated flames are statistically one-dimensional and provides the various local mean quantities of interest as a function of time t and

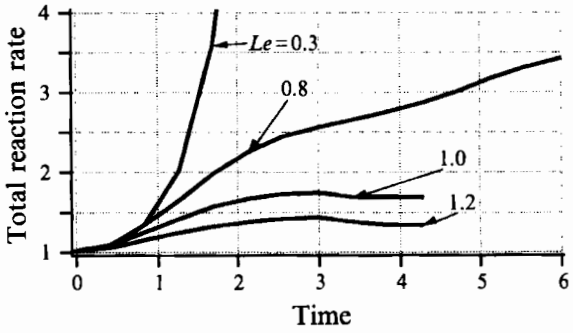

FIGURE 3. Lewis-number effects on the overall reaction rate. The total reaction rate, $\overline{\langle \dot{\omega}_R \rangle}$, is made non-dimensional by its initial value corresponding to a strain-free plane laminar flame. Time is made non-dimensional by the initial turbulent eddy turnover time, τ_0.

position x within the turbulent flame brush. In the present case, (5), (6) and (7) translate to the following relations:

$$\widehat{S_C}(t) = \left(\int \langle S_C \rangle_S(x,t)\, \Sigma(x,t)\, \mathrm{d}x \right) \Big/ \left(\int \Sigma(x,t)\, \mathrm{d}x \right), \tag{34}$$

$$\frac{\langle S_V \rangle(t)}{L_y L_z} = \int \Sigma(x,t)\, \mathrm{d}x, \tag{35}$$

$$S_T(t) = \frac{1}{\rho_u Y_{R,u}} \int \langle \dot{\omega}_R \rangle(x,t)\, \mathrm{d}x = \widehat{S_C}(t) \frac{\langle S_V \rangle(t)}{L_y L_z}. \tag{36}$$

In (34), if the computational domain is large enough and space-averaging can be used to obtain ensemble-averages, then the mean fuel consumption speed, $\widehat{S_C}$, can also be expressed as the area-weighted space-averaged value of S_C integrated along the turbulent flame surface: $\widehat{S_C} = \int S_C\, \delta A / \int \delta A$, where δA designates the area of an infinitesimal flame element and where integration takes places along the flame contour. This last expression does not require an estimate of the flame surface density and was previously used by Haworth & Poinsot (1992).

Another useful global flame property is the total flame stretch, $\hat{\kappa}$. Using (12), $\hat{\kappa}$ can be directly related to the instantaneous rate of change of the total flame surface area in the computational domain:

$$\hat{\kappa}(t) \equiv \left(\int \langle \kappa \rangle_S(x,t)\, \Sigma(x,t)\, \mathrm{d}x \right) \Big/ \left(\int \Sigma(x,t)\, \mathrm{d}x \right) = \frac{\mathrm{d}\langle S_V \rangle}{\mathrm{d}t} \Big/ \langle S_V \rangle. \tag{37}$$

If $\hat{\kappa}$ is positive, the flame surface grows; if negative, the flame surface contracts.

As described in §3, four different cases have been simulated that correspond to turbulent flames characterized by the same laminar flame thickness, l_F, the same laminar flame speed, s_L, embedded in the same initial turbulent flow field, but with different Lewis number, $Le = 0.3$, 0.8, 1.0 and 1.2.

Figure 3 shows that the four cases exhibit large differences in the time history of the total reaction rate, $\overline{\langle \dot{\omega}_R \rangle}(t)$. These differences remain moderate when comparing $Le = 1.0$ and 1.2. They are much stronger for $Le = 0.8$: after 4 turbulent eddy turnover times, $t/\tau_0 > 4$, the $Le = 0.8$ flame burns twice as fast as the $Le = 1.2$ flame. And they prove quite dramatic for $Le = 0.3$: after only 2 eddy turnover times, $t/\tau_0 > 2$, the $Le = 0.3$ flame burns more than twice as fast as the $Le = 0.8$ flame. In fact, the

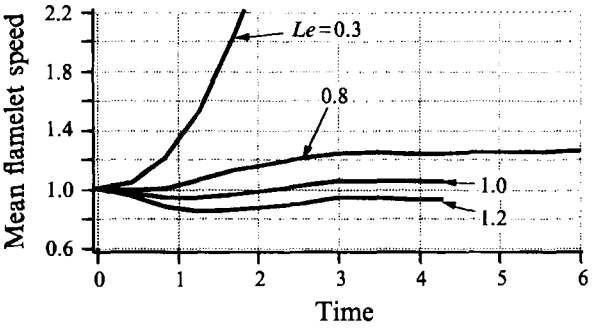

FIGURE 4. Lewis-number effects on the mean fuel consumption speed, $\widehat{S_C}$. $\widehat{S_C}$ is made non-dimensional by the laminar flame speed, s_L. Time is made non-dimensional by the initial, turbulent eddy turnover time, τ_0.

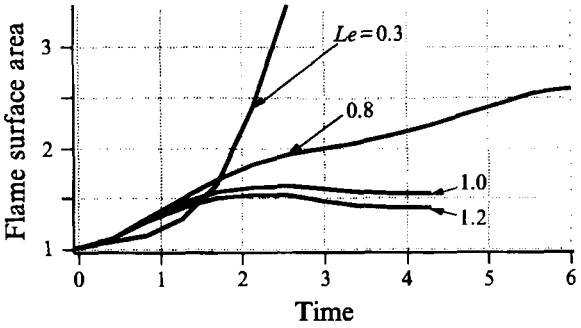

FIGURE 5. Lewis-number effects on the relative increase of total flame surface area, $\langle S_V \rangle / L_y L_z$. Time is made non-dimensional by the initial, turbulent eddy turnover time, τ_0.

acceleration of the $Le = 0.3$ flame is so dramatic that the computations have to be stopped at $t/\tau_0 \approx 2.5$, as the first flame elements have already reached the left-hand side of the computational domain.

The sensitivity of the global flame response to changes in the flame physical properties has been the focus of a number of recent experimental studies. Strong thermo-diffusive effects, similar to the present results, have been observed in turbulent flames both at low Reynolds numbers (Lee, North & Santavicca 1992; Goix & Shepherd 1992) and high Reynolds numbers (Abdel-Gayed *et al.* 1984; Wu *et al.* 1990). For instance, Wu *et al.* (1990) show that a turbulent hydrogen–air jet flame, characterized by $Re_l \approx 1800, u'/s_L \approx 3$, and unstable thermo-diffusive conditions ($Le < 1$), has twice the turbulent flame speed of a similar flame but with stable thermo-diffusive conditions ($Le > 1$).

As suggested by (36), such differences in the flame response may be related to a modification of the turbulent flame structure through changes in $\widehat{S_C}$, to a modification of the total flame surface area through changes in $\langle S_V \rangle$, or to a combination of both. The effect of the Lewis number on the mean turbulent flame structure is shown in figure 4. For flames with Lewis numbers close to unity, $0.8 \leqslant Le \leqslant 1.2$, the mean flamelet speed, $\widehat{S_C}$, is found to be only a weak function of the turbulence: at all times, departures of $\widehat{S_C}$ from the laminar value, s_L, remain within 30%. In contrast to these flames, when $Le = 0.3$, the mean combustion intensity is strongly amplified, $\widehat{S_C}$ grows exponentially and, at $t/\tau_0 > 2$, takes values that are more than twice as large as s_L.

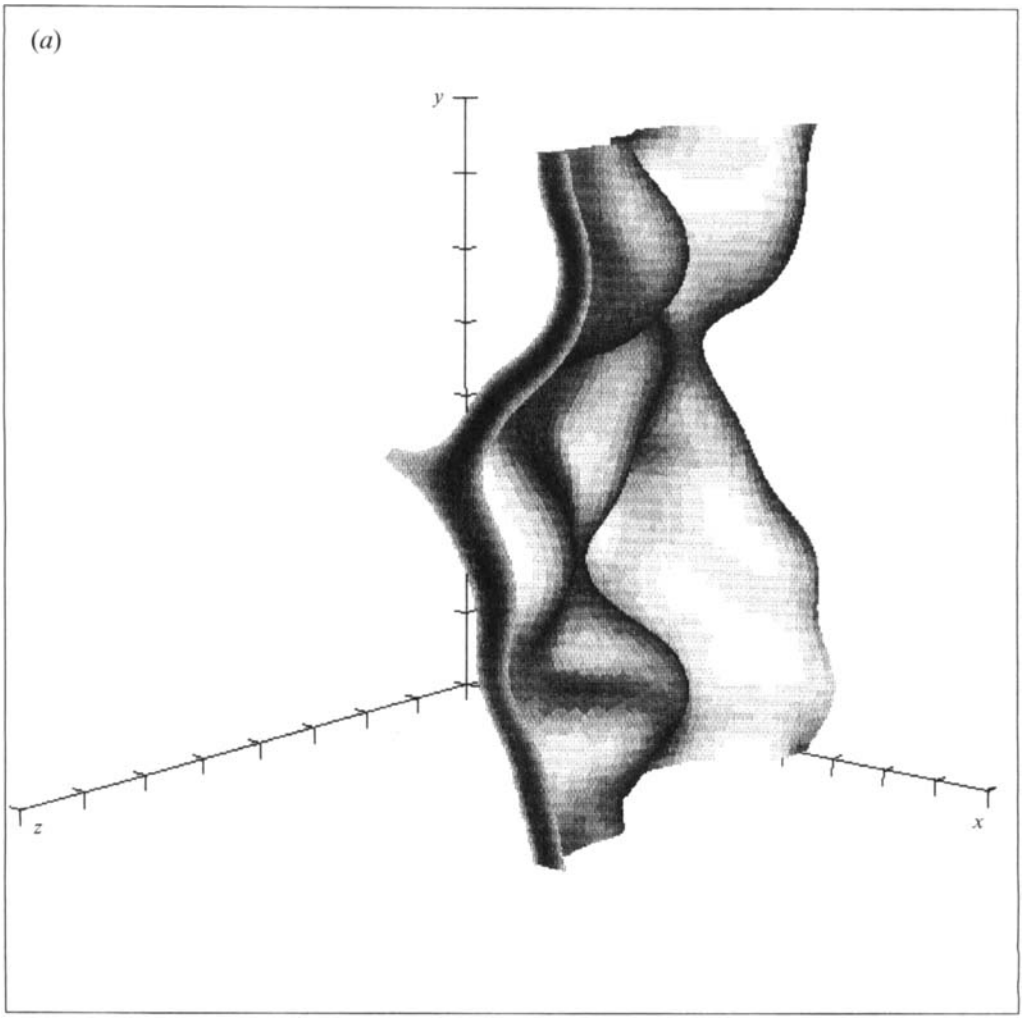

FIGURE 6(*a*). For caption see page 17.

The effect of the Lewis number on flame surface production is presented in figure 5. For $Le = 1.0$ and 1.2, the flame surface area initially increases, reaches a maximum, and then decreases in time. The increase occurs as the turbulence wrinkles the initially flat flame surface. The flame then adapts to its turbulent environment, and, as the turbulence decays, the flame surface becomes smoother and relaxes to its initial state. The $Le = 0.3$ and 0.8 flames exhibit a strikingly different behaviour where the flame surface area keeps increasing in time without saturation. Although saturation might be expected at later times, our simulations are limited by the size of the computational domain and this subsequent phase is not observed. In any case, the simulations indicate that saturation will not occur on a timescale characteristic of the turbulence. In that sense, the $Le = 0.3$ and 0.8 flames can be qualified as unstable.

As might be expected, the differences between stable and unstable burning are so pronounced that one can easily detect the transition from one regime to the other by comparing instantaneous snapshots of the flame surface (figure 6). For instance, for $Le = 0.3$ or 0.8, fingers of burnt products are seen to propagate at a fast rate into the fresh reactants (figures 6*d* and 6*c*). We believe that this 'fingering' is an important

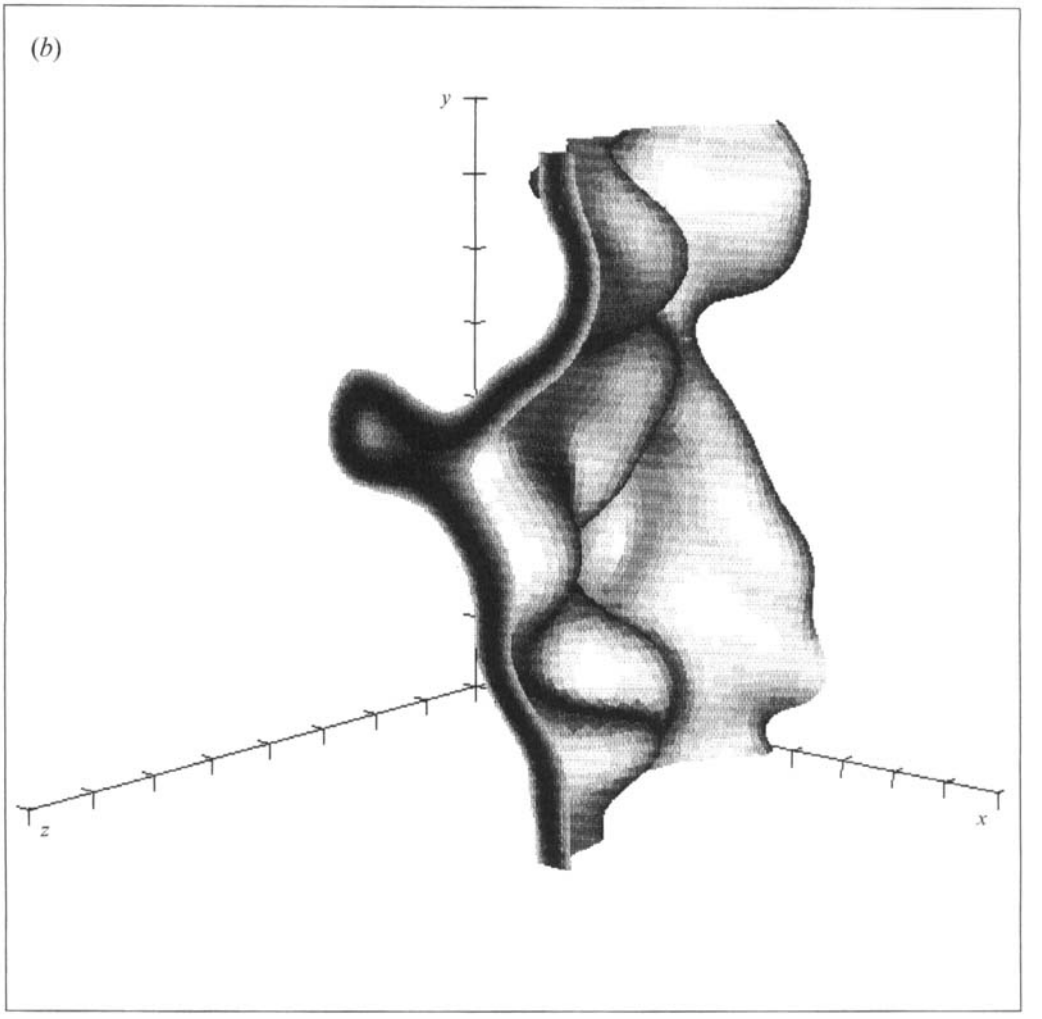

FIGURE 6(*b*). For caption see page 17.

ingredient of the flame instability process and of the overall flame acceleration. The 'fingering' is not observed in the $Le = 1.0$ or 1.2 flames (figures 6*b* and 6*a*).

In summary, when interpreting the global flame response, it is useful to distinguish the $Le = 0.3$ case from the other cases where the Lewis number is close to unity, $0.8 \leqslant Le \leqslant 1.2$. For flames with Lewis numbers close to unity, our results are in agreement with previous findings by Ashurst *et al.* (1987), Haworth & Poinsot (1992), Rutland & Trouvé (1993). In these studies, the effect of the Lewis number on the turbulent flame speed, S_T, is shown to be primarily a flame surface effect. The modelling implications of this result are that for nearly equi-diffusive mixtures, the variations in the flame structure due to the turbulence can be neglected and the flame surface density is the single key quantity that to first order determines the mean reaction rate. Our results, however, also show that these conclusions are Lewis-number dependent and suggest that they might in fact only hold for Lewis numbers in a finite range around $Le = 1$. In the $Le = 0.3$ case, the dramatic effect of the Lewis number on flame surface production is coupled with a significant increase in the mean flame intensity. Therefore, for mixtures characterized by a strong imbalance in diffusive properties, both the flame

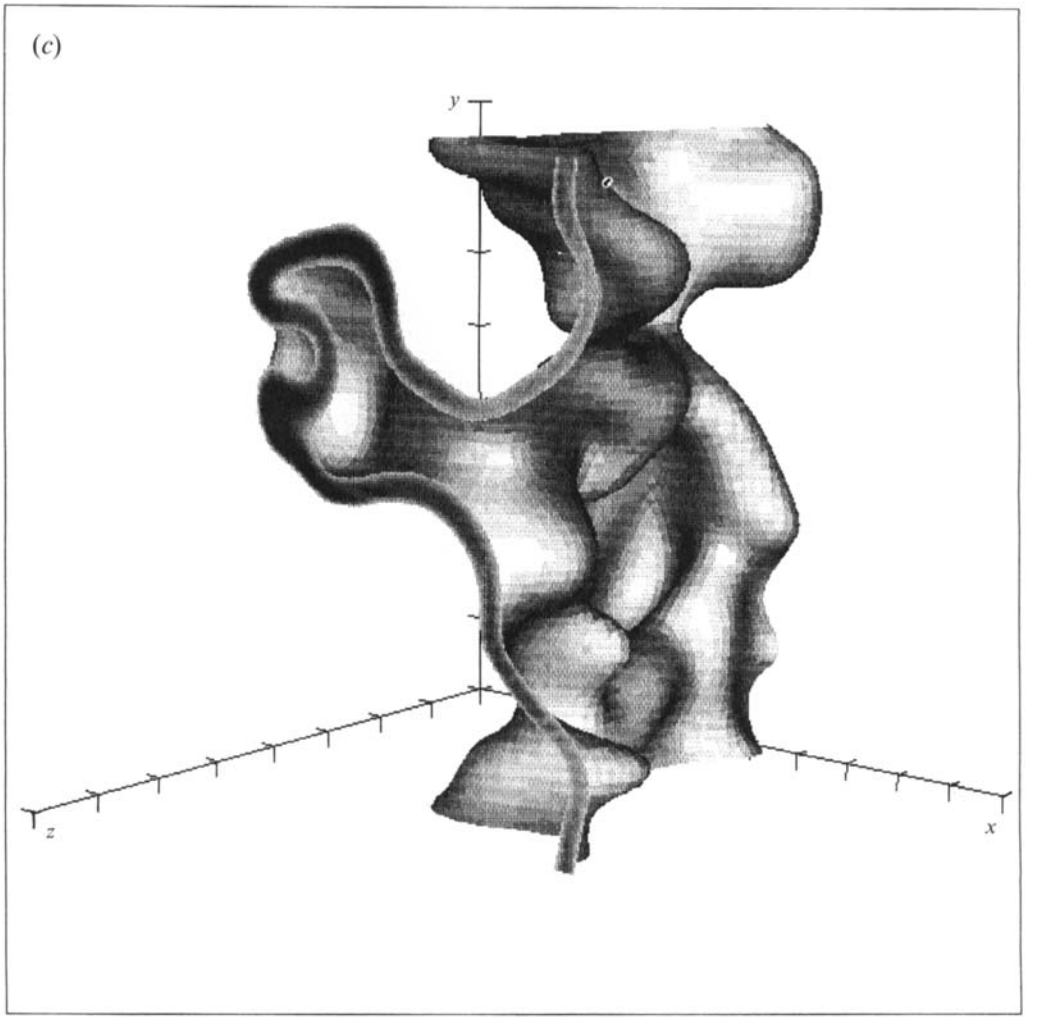

FIGURE 6(c). For caption see facing page.

surface density and the flamelet speed need to be modelled to determine the mean reaction rate.

4.2. *Local flame properties*

4.2.1. *The flame surface density profiles*

Using the methodology described in §3.2, we now analyse the spatial distribution of flame surface density across the turbulent flame brush. Figure 7 compares several Σ-profiles taken at different instants in the simulations. The Lewis number is 0.8. At $t = 0$, Σ is a Dirac delta-function located at $x = 0$. As time evolves, the turbulent flame brush grows thicker and propagates deeper into the reactants. Accordingly, the Σ-profile spreads out and shifts towards negative values of x. In figure 7, this shift is rather weak but becomes more visible as time increases.

Figure 8(*a*) compares the Σ-profiles obtained for different Lewis numbers. The comparison is performed at the same instant in the simulations, $t/\tau_0 \approx 4.3$. The effect of the Lewis number is clearly seen in figure 8(*a*) with a turbulent flame brush that propagates faster and deeper into the reactants for more diffusive mixtures. Note that,

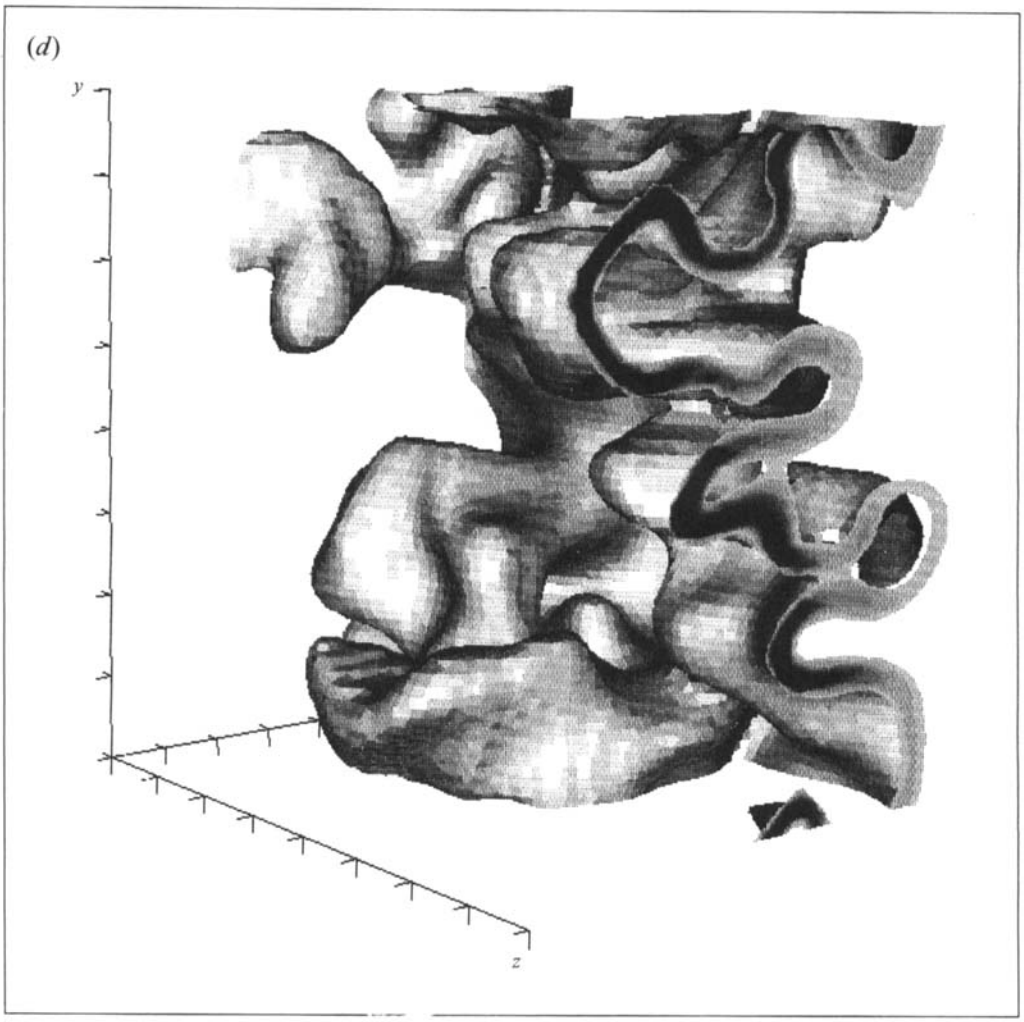

FIGURE 6. Snapshots of the flame surface contour, $c = c_f$: (*a*) $Le = 1.2$; (*b*) $Le = 1.0$; (*c*) $Le = 0.8$; (*d*) $Le = 0.3$. While pictures (*a*), (*b*) and (*c*) are taken at time $t/\tau_0 \approx 4.3$ and show a perspective where the flow is from top-left (reactants) to bottom-right (products), picture (*d*) is taken at an earlier time, $t/\tau_0 \approx 2.5$, and shows a different perspective where the flow is from bottom-left (reactants) to top-right (products).

as shown in (35), the x-integral of Σ gives the relative increase of total flame surface area and the local differences in the profiles plotted in figure 8(*a*), when integrated, correspond to large global differences in the total amount of flame surface area, $\langle S_V \rangle$.

A different perspective is adopted in figure 8(*b*) where x-location within the turbulent flame brush is indicated by the local mean progress variable, $\langle c \rangle$; $\langle c \rangle(x, t)$ versus x is a monotonic bounded profile and the thickness of this profile is the turbulent flame thickness, δ_t. Although they are different in physical space, the Σ-profiles obtained for different Lewis numbers collapse when mapped in $\langle c \rangle$-space. This result indicates that the effect of the Lewis number on the spatial distribution of flame surface density, as observed in the simulations, is primarily an effect on δ_t.

Also plotted in figure 8(*b*) is the flame surface density predicted by the Bray–Moss–Libby (BML) model. This curve will be discussed in §5.1.

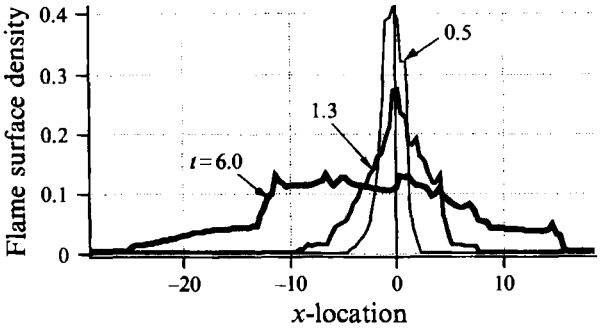

FIGURE 7. Time evolution of the flame surface density, Σ, in the computational domain (reactants on the left; products on the right). $Le = 0.8$. Σ and x are made non-dimensional by the laminar flame thickness, l_F. t is measured in units of the initial turbulent eddy turnover time, τ_0.

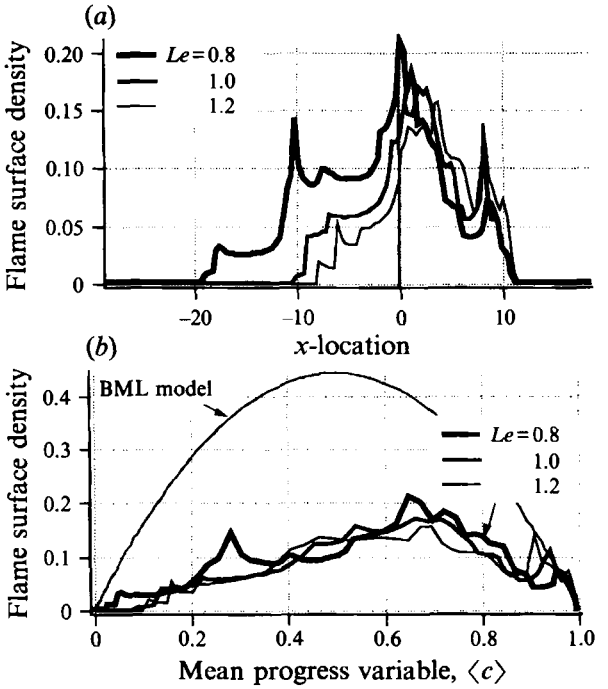

FIGURE 8. The spatial distribution of flame surface density, Σ, across the turbulent flame brush: (*a*) in physical space; (*b*) in $\langle c \rangle$-space, where DNS results are compared with the Bray–Moss–Libby model. $t/\tau_0 \approx 4.3$. Σ and x are made non-dimensional by the laminar flame thickness, l_F.

4.2.2. *The source and sink terms in the equation for* Σ

One important advantage of the present analysis is to distinguish between the leading edge and the rear edge of the turbulent flame brush. The geometry as well as the dynamics of the flame differ quite significantly from one end of the reaction zone to the other, as shown in figures 9–15. For convenience in the next plots we adopt the perspective of figure 8(*b*), where location within the turbulent flame brush is indicated by $\langle c \rangle$ instead of x. Also, all the plotted profiles in this subsection are instantaneous. While these profiles do vary in the course of the simulations, we are only interested here in their persistent features, i.e. their basic properties that are independent of the

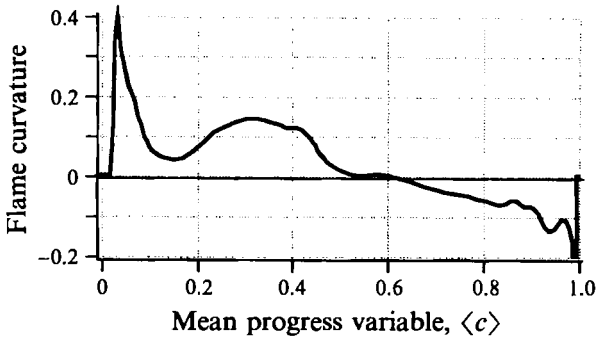

FIGURE 9. Variations of the mean flame curvature, $\langle k_m \rangle_S$, across the turbulent flame brush. $Le = 0.8$, $t/\tau_0 \approx 4.3$. Flame curvature is made non-dimensional by the laminar flame thickness, l_F.

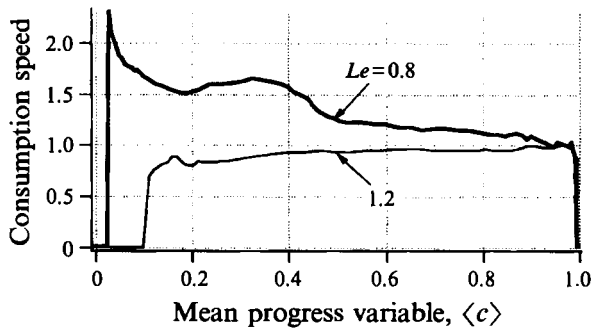

FIGURE 10. Variations of the mean fuel consumption speed, $\langle S_C \rangle_S$, across the turbulent flame brush. $t/\tau_0 \approx 4.3$. S_C is made non-dimensional by the laminar flame speed, s_L.

turbulence decay. These persistent features were determined by a systematic analysis of the database. Finally, except for the $Le = 0.3$ case, comparisons between the different simulations are performed at normalized time $t/\tau_0 \approx 4.3$, when the flame response to the turbulence is fully developed. Since the flame response is much faster for $Le = 0.3$, data are in that case analysed at an earlier time, $t/\tau_0 \approx 2.5$. The values of the turbulent length and velocity scales at these instants are reported in table 2.

Figure 9 presents the spatial variations of the mean flame curvature, $\langle k_m \rangle_S$, across the reaction zone. The mean curvature goes from positive at the leading edge to negative at the rear edge of the turbulent flame. Since in non-unity-Lewis-number flames, the local flame intensity, as measured by the fuel consumption speed, S_C, depends strongly on flame curvature, and since the dependence is quasi-linear (Haworth & Poinsot 1992; Rutland & Trouvé 1993), the strong variations in mean flame geometry illustrated by figure 9 must correspond to equally strong variations in mean flame structure. Moreover, since the correlation between S_C and k_m is Lewis-number dependent (positive for $Le < 1$ and negative for $Le > 1$), the spatial variations of the flamelet speed, $\langle S_C \rangle_S$, are expected to show opposite trends for $Le = 0.8$ and 1.2. Figure 10 shows that this is indeed the case. For $Le = 0.8$, $\langle S_C \rangle_S$ is like $\langle k_m \rangle_S$ a decreasing function of the mean progress variable, $\langle c \rangle$. In that case, the combustion intensity at the leading edge is higher than at the rear edge of the turbulent flame. On the other hand, for $Le = 1.2$, the flame structure goes from slower burning, close to $\langle c \rangle = 0$, to faster burning, close to $\langle c \rangle = 1$. Note that the magnitude of the variations in $\langle S_C \rangle_S$ is much decreased for $Le = 1.2$ compared to $Le = 0.8$. For $Le = 1$, $\langle S_C \rangle_S$ remains approximately constant and equal to the laminar flame speed, s_L.

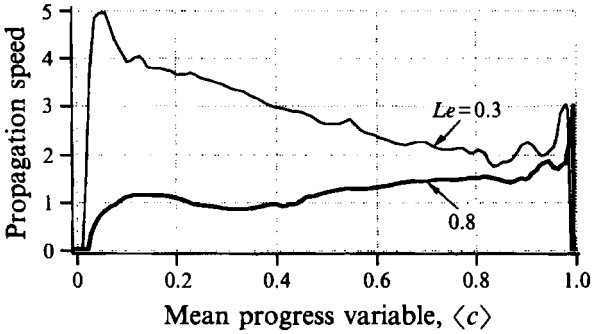

FIGURE 11. Variations of the mean flame propagation speed, $\langle w \rangle_s$, across the turbulent flame brush. Note that while the $Le = 0.8$ curve uses data taken at time $t/\tau_0 \approx 4.3$, the $Le = 0.3$ curve corresponds to an earlier time, $t/\tau_0 \approx 2.5$. w is made non-dimensional by its value corresponding to a strain-free plane laminar flame, $w = s_L \rho(c = 0)/\rho(c = c_f)$.

Our discussion of the flamelet framework in §§1 and 2 indicates that in the flamelet regime, a flame element can be characterized by two speeds: a chemical rate, S_C, and a kinematic quantity, w. We recall that w gives the velocity of the flame front with respect to the flow field and is measured at $c = c_f$, where reaction actually occurs, $w \equiv w(c = c_f)$. A more familiar quantity is the flame displacement speed relative to the unburnt gas. This speed is defined at the upstream boundary of the preheat zone, $S_d \equiv w(c = 0^+)$. For a steady strain-free plane laminar flame, the speeds S_C and S_d are the same and are equal to s_L, while w accounts for the flow acceleration due to density variations, $w = s_L \rho(c = 0)/\rho(c = c_f)$. For unsteady flames, however, or flames subjected to stretch, that is strained and/or curved, these simple one-dimensional relations no longer hold. For instance, at the tip of a Bunsen burner, the speeds S_C and S_d, as well as S_C and w, can differ by an order of magnitude (Poinsot, Echekki & Mungal 1992).

In fact, situations might occur where the rate of fuel consumption and the rate of flame propagation not only prove to be different but also exhibit opposite behaviour. This richness and subtlety in the flame response is illustrated in figure 11. A comparison of figures 10 and 11 indicates that for $Le = 0.8$, the leading edge of the turbulent flame burns faster but propagates more slowly than the rear edge of the flame, which burns more slowly but propagates faster into the reactants.

This paradox is similar to that occurring in stretched laminar flames for Lewis numbers slightly below one. For instance, for weak stretch the classical theory of laminar flames predicts a linear response for the influence of stretch, κ, on both the displacement speed, S_d, and the fuel consumption speed, S_C (Clavin & Williams 1982; Pelcé & Clavin 1982; Clavin 1985; Williams 1985):

$$S_d = s_L - \mathscr{L}_d \kappa, \tag{38}$$

$$S_C = s_L - \mathscr{L}_C \kappa, \tag{39}$$

where $\mathscr{L}_d$ is a constant known as the Markstein length, and $\mathscr{L}_C$ is another constant, sometimes designated as a second Markstein length. Both $\mathscr{L}_d$ and $\mathscr{L}_C$ are functions of the flame physical properties. They are, in particular, functions of the Lewis number and change sign at some critical value of Le, going from positive to negative as Le decreases. These critical values, however, are different: while $\mathscr{L}_C$ changes sign at $Le = 1$, $\mathscr{L}_d$ changes sign at a different value, $Le = Le_c$ (see table 3). Le_c is called the critical Lewis number and its value for practical laminar flames is below one (Clavin & Garcia 1983). As pointed out in the studies by Matalon & Matkowsky (1982) and Matalon

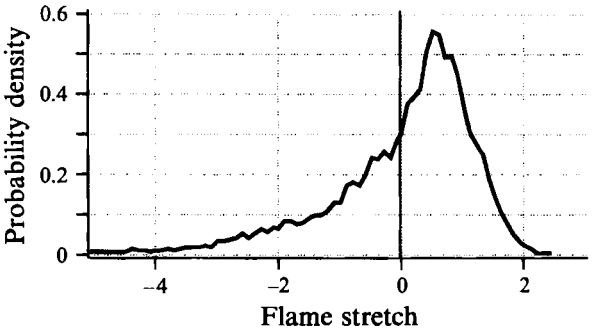

FIGURE 12. Probability density function of flame stretch, κ, measured at the flame surface, $c = c_f$. $Le = 0.8$, $t/\tau_0 \approx 4.3$. Stretch is made non-dimensional by the laminar flame time, $(\lambda_{th}/\rho c_p)_u/s_L^2$.

Le	$\mathscr{L}_d$	$\mathscr{L}_C$
0	−	−
Le_c	0	−
1.0	+	0
∞	+	+

TABLE 3. Lewis-number effects on the sign of the Markstein lengths, $\mathscr{L}_d$ and $\mathscr{L}_C$. $\mathscr{L}_d$ and $\mathscr{L}_C$ are respectively based on the flame displacement speed, S_d, and the fuel consumption speed, S_C, see (38) and (39)

(1983), the local flame response may then be summarized as follows: when $1 < Le$, a positive (negative) stretch tends both to reduce (increase) the flame intensity and slow down (speed up) the flame; when $Le_c < Le < 1$, an increase (decrease) in flame intensity occurs for $\kappa > 0$ ($\kappa < 0$) together with a decrease (increase) in the flame displacement speed; when $Le < Le_c$, a positive (negative) stretch increases (reduces) the flame intensity and accelerates (decelerates) the flame. The interesting prediction here is that the effects of stretch on flame structure and flame propagation are opposite in the range $Le_c < Le < 1$.

While these theoretical results are formally limited to weak stretch, they do not require the flow to be laminar and the Markstein length remains a valid concept in turbulent flames with large scales and low intensities (Clavin & Williams 1982; Aldredge & Williams 1991). For more general cases, the weak stretch theory still provides a useful framework for interpreting the dynamics of flamelets embedded in turbulent flows. For instance, the surprising result in the simulations that when $Le = 0.8$, an increase in flame intensity is not necessarily associated with an acceleration of the flame (figures 10 and 11) is consistent with Lewis-number effects in the weak stretch theory and a critical Lewis number in the range $0.3 < Le_c < 0.8$. On the other hand, some other results from the simulations are found to be at odds with the theory. For instance, the properties of individual flame elements seem to correlate with flame curvature rather than flame stretch. Similar observations emphasizing the role of curvature were made in previous studies by Haworth & Poinsot (1992) and Rutland & Trouvé (1993). This interesting point is beyond the scope of the present paper and will be addressed in future work. Also, while the data suggest that the critical Lewis number is above 0.3, an estimate of Le_c based on the theoretical expression proposed by Clavin & Garcia (1983) gives $Le_c \approx 0.1$. As shown in figure 12, the DNS values of κ, at time $t/\tau_0 \approx 4.3$, range from -5 to 2 (in units of the laminar flame time). These values of

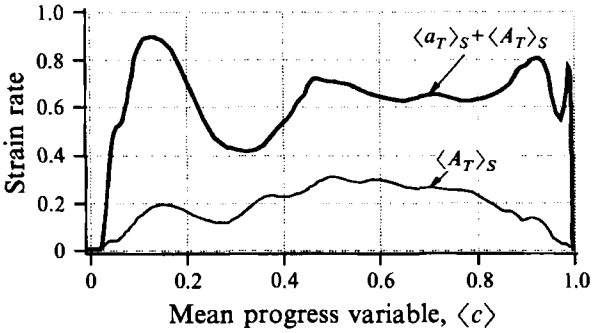

FIGURE 13. Variations of the mean strain rate across the turbulent flame brush. While $\langle A_T\rangle_S$ represents the effect of the mean flow gradient, $\langle a_T\rangle_S+\langle A_T\rangle_S$ is the total mean strain rate, see (14) and (15). $Le = 0.8, t/\tau_0 \approx 4.3$. Strain rate is made non-dimensional by the laminar flame time, $(\lambda_{th}/\rho c_p)_u/S_L^2$.

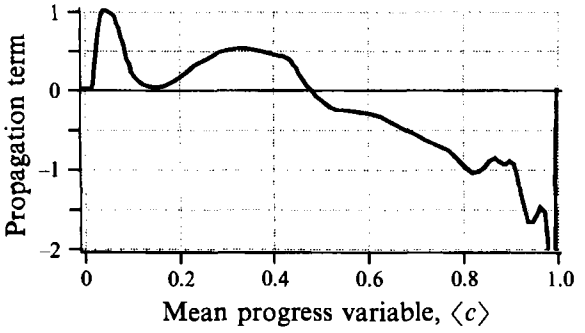

FIGURE 14. Variations of the mean propagation term, $2\langle wk_m\rangle_S$, across the turbulent flame brush. $Le = 0.8, t/\tau_0 \approx 4.3$. wk_m is made non-dimensional by the laminar flame time, $(\lambda_{th}/\rho c_p)_u/s_L^2$.

stretch are quite large and the simulated flames are clearly beyond the domain of validity of the weak stretch theory, which might account for the apparent discrepancies.

We now turn to the terms appearing on the right-hand side of the equation for Σ. As seen in (14) and (15), the mean tangential strain rate at the flame can be decomposed into two components. Both components are presented in figure 13. The strain rate due to the mean flow field is a production term and depends on the mean streamwise velocity gradient and the flamelet orientation: $\langle A_T\rangle_S = (1-\langle n_x^2\rangle_S)\,\mathrm{d}\tilde{U}/\mathrm{d}x$, where n_x is the x-component of the flame normal vector. In fact, the simulations indicate that the statistics describing the flamelet orientation do not vary significantly across the turbulent brush (see §5.1), and $\langle A_T\rangle_S$ may be considered as proportional to $\mathrm{d}\tilde{U}/\mathrm{d}x$. The turbulent component, $\langle a_T\rangle_S$, is also a production term. In the mean, globally as well as locally, the turbulent motions always tend to increase the flame surface area.

While the total strain term, $\langle a_T\rangle_S+\langle A_T\rangle_S$, remains positive and approximately constant across the turbulent flame, the propagation term, $2\langle wk_m\rangle_S$, exhibits strong spatial variations and decreases from positive values on the unburnt side, close to $\langle c\rangle = 0$, to negative values on the burnt side, close to $\langle c\rangle = 1$ (figure 14). Thus, while the propagation term is the only term in the transport equation for Σ that accounts for dissipation of flame surface area, its role is not constant across the flame zone and switches from production at the front to dissipation at the back.

The net effect on the surface growth rate is given by the flame stretch, $\langle\kappa\rangle_S = (\langle a_T\rangle_S+\langle A_T\rangle_S)+2\langle wk_m\rangle_S$, and is presented in figure 15(*a*). Interestingly, a

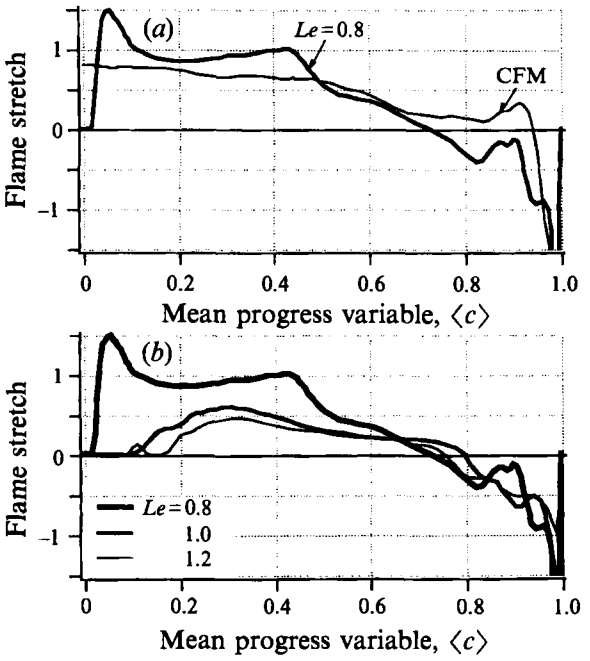

FIGURE 15. Variations of the mean flame stretch, $\langle \kappa \rangle_S$, across the turbulent flame brush: (*a*) comparison between DNS results ($Le = 0.8$) and the coherent flame model; (*b*) Lewis-number effects (DNS results). $t/\tau_0 \approx 4.3$. Stretch is made non-dimensional by the laminar flame time, $(\lambda_{th}/\rho c_p)_u/s_L^2$.

comparison of figures 13 and 14 indicates that both contributions to stretch – total strain and propagation – have the same order of magnitude. At the leading edge of the reaction zone, strain rate and flame propagation effects are locally cumulative and the overall balance is strongly positive. The leading edge of the turbulent flame is a region of strong production of flame surface area. On the other hand, the propagation term takes large negative values on the burnt side. In that region, strain rate and flame propagation effects are locally opposite and the overall balance is negative. The rear edge of the turbulent flame thus appears as a region where flame surface area gets strongly dissipated.

Also plotted in figure 15(*a*) is the turbulent flame stretch predicated by the coherent flame model (CFM). This model and its performance compared to the DNS results will be discussed in § 5.2.

Figure 15(*b*) presents the mean flame stretch profiles, $\langle \kappa \rangle_S$ versus $\langle c \rangle$, plotted for different Lewis numbers. In all cases, stretch takes large negative values on the burnt side, close to $\langle c \rangle = 1$. The effect of the Lewis number is not significant in that region. In comparison, at the leading edge of the flame, large differences between the different Lewis number cases appear. This suggests that the turbulent flame is most sensitive to Lewis-number effects on the unburnt side, whereas it remains relatively unaffected on the burnt side.

The stretch profiles spatially resolve the balance between production and dissipation of flame surface area. The net global growth rate is given by the total flame stretch, $\hat{\kappa}$, as defined in (37). At time $t/\tau_0 \approx 4.3$, we find (in units of the laminar flame time) the following: $\hat{\kappa} = 1.2$ for $Le = 0.8$, and the flame surface area is quickly growing; $\hat{\kappa} = 0.1$ for $Le = 1.0$, and $\hat{\kappa} \approx 0$ for $Le = 1.2$, and the flame surface area remains approximately constant.

5. Comparisons of DNS results with flamelet models

5.1. *Models based on algebraic closures*

The flame surface density profiles presented in §4.2.1 can be directly compared to the predictions by the Bray–Moss–Libby (BML) model. The BML model is a well-documented second-order closure model designed to avoid gradient transport assumptions (Bray 1980, 1990; Bray *et al.* 1989). The model assumes a bimodal shape for the probability density function of the progress variable, an assumption that is consistent with a flamelet description of the reaction zone and represents the intermittent presence of packets of unburnt and fully burnt mixture at any location within the turbulent flame brush.

Various degrees of refinement are possible within the BML framework, in particular with respect to the chemical source terms and the flame surface density. Although a transport equation for Σ could be incorporated easily (Cant *et al.* 1990), current formulations of the model are limited to a simple algebraic closure (Bray *et al.* 1984, 1989). The key quantity in this closure is the flamelet crossing frequency, n_y, defined as the number of crossings of the flame surface, $c = c_f$, per unit distance along a contour, $\langle c \rangle = \text{constant}$; n_y is obviously a function of $\langle c \rangle$. In the present one-dimensional problem, the expression for n_y in a (y,z)-plane, $x = x_0$, where $\langle c \rangle = \text{constant}$, is

$$n_y = \frac{\displaystyle\int_{c=c_f} \mathrm{d}l}{L_y L_z}, \tag{40}$$

and, combining (30) and (40), we can write

$$\Sigma = \frac{\displaystyle\int_{c=c_f} \mathrm{d}l}{L_y L_z} \times \frac{\displaystyle\int_{c=c_f} \mathrm{d}l/|\cos\theta|}{\displaystyle\int_{c=c_f} \mathrm{d}l} = n_y \times \frac{1}{\bar{\sigma}_y}, \tag{41}$$

where $\bar{\sigma}_y$ is the mean of a direction cosine defining the flamelet orientation relative to the plane, $x = x_0$ (see figure 2):

$$\bar{\sigma}_y = \frac{\displaystyle\int_{c=c_f} \mathrm{d}l}{\displaystyle\int_{c=c_f} \mathrm{d}l/|\cos\theta|} = \langle |\cos\theta| \rangle_S. \tag{42}$$

Equation (41) is an exact relation and the flame surface density can always be written as the flamelet crossing frequency, n_y, divided by a flamelet orientation factor, $\bar{\sigma}_y$. Using this decomposition, the closure problem for Σ requires tractable expressions for n_y and $\bar{\sigma}_y$. In the BML model, $\bar{\sigma}_y$ is assumed to be a universal constant, so that the physical processes that control the flame surface dynamics are represented exclusively through the flamelet crossing frequency. The flamelet crossing frequency is obtained by a statistical analysis of the transitions between burnt and unburnt states. The BML expressions for n_y and Σ are

$$n_y = \frac{g\langle c \rangle (1 - \langle c \rangle)}{\hat{L}_y}, \quad \Sigma = \frac{g\langle c \rangle (1 - \langle c \rangle)}{\bar{\sigma}_y \hat{L}_y}, \tag{43}$$

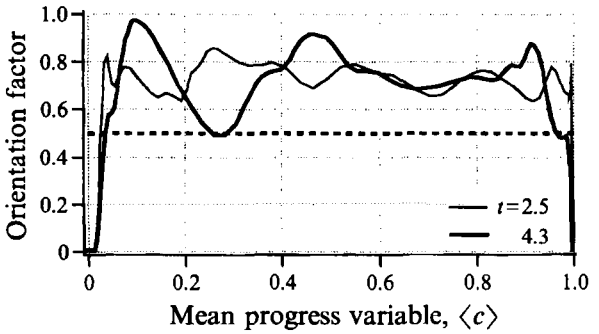

FIGURE 16. Variations of the flamelet orientation factor, $\bar{\sigma}_y$, across the turbulent flame brush. Le = 0.8. The dashed line is the Bray–Moss–Libby prediction. t is measured in units of the initial turbulent eddy turnover time, τ_0.

where g is a constant of order unity, and $\hat{L}_y$ is a length that characterizes the flame wrinkling. Finally, $\hat{L}_y$ is assumed to be constant across the turbulent flame brush and is specified empirically as follows:

$$\hat{L}_y = C_L l(s_L/u')^n, \tag{44}$$

where C_L and n are model constants.

It is worth emphasizing that in general, as suggested by (30), measuring the flame surface density requires knowledge of the three components of ∇c at the flame, i.e. requires access to three-dimensional spatial information. The first merit of the BML formulation for the mean reaction rate is to relate the flame surface density to a quantity n_y, which, as seen in (40), can be measured in planes. The three-dimensional information is conveyed by the flamelet orientation factor, $\bar{\sigma}_y$, and $\bar{\sigma}_y$ is assumed to be a constant. This assumption is of great practical significance since it puts Σ at the level of n_y, i.e. at an experimentally accessible level. In experiments, (40) can be evaluated via, for example, laser tomography techniques (Driscoll & Gulati, 1988; Cheng, Shepherd & Talbot 1988; Chew, Bray & Britter 1990).

The assumption, $\bar{\sigma}_y$ = constant, is tested in figure 16 where $\bar{\sigma}_y$, is plotted across the turbulent flame brush, at two different instants, $t/\tau_0 \approx 2.5$ and $t/\tau_0 \approx 4.3$. As seen in figure 16, and irrespective of the value of the Lewis number, the flamelet orientation factor computed from the simulations is found to be approximately constant, both in space and time, $\bar{\sigma}_y \approx 0.7$. This result is in excellent agreement with the BML formulation and suggests that a simple expression like (40) can be used instead of the exact expression (30) to calculate the flame surface density. Note that the DNS value for $\bar{\sigma}_y$ is slightly higher than the value proposed by Bray (1990), $\bar{\sigma}_y = 0.5$.

The result, $\bar{\sigma}_y$ = constant, however, does not lead to a better model for Σ because of uncertainties over an appropriate description for the flamelet crossing frequency. A comparison of the BML expressions (43) and (44) with the DNS-based Σ-profiles is presented in figure 8(*b*). Following Bray (1990), we use for the model constants: $n = 1, C_L = 1, g = 1.5, \bar{\sigma}_y = 0.5$. Figure 8(*b*) shows that the structure of the Σ-profile is not accurately captured by the BML model. The model predicts a symmetric distribution of flame surface density in $\langle c \rangle$-space, whereas the simulations generate skewed profiles with a maximum close to $\langle c \rangle = 0.7$. These DNS results are consistent with previous experimental studies by Driscoll & Gulati (1988), Cheng *et al.* (1988), and Chew *et al.* (1990), where the variations of the flamelet crossing frequency across the flame were found to be asymmetric and skewed towards the burnt gas.

Furthermore, although the comparison between DNS data and the BML model is rendered difficult by the turbulence decay, some qualitative observations can still be made about the general accuracy or inaccuracy of the model. For instance, the BML predictions always overestimate the flame surface densities across the turbulent flame brush, by a factor decreasing from more than 5 to approximately 2 in the course of the simulations. Although the exact magnitude of the error might not be meaningful, the fact that it is time-dependent underscores the limits of an algebraic closure that cannot account for memory effects and is therefore expected to perform poorly in transient problems. These observations suggest that a more complete description might be required.

5.2. *Models based on the turbulent Σ-equation*

The flamelet models based on the turbulent Σ-equation offer a more complex, but also more complete and more promising approach. As discussed in the introduction, different formulations of the modelled Σ-equation may be found in the literature. We choose to consider in this section the coherent flame model (CFM), based on the ideas originally proposed by Marble & Broadwell (1977), and later developed by Candel and his co-workers (Darabiha *et al.* 1987; Maistret *et al.* 1989; Candel *et al.* 1990). Also, for clarity, we limit our discussion to an early version of CFM. More elaborate formulations of CFM and comparisons with other flamelet models may be found in Duclos *et al.* (1993). Our objective here is not to provide a final evaluation of these models but to demonstrate the usefulness of DNS in performing such an evaluation.

In CFM, the balance equation for Σ is written as

$$\frac{\partial \Sigma}{\partial t} + \nabla \cdot \tilde{U}\Sigma = \nabla \cdot \{D_t \nabla \Sigma\} + \left\{ C_1 \frac{\epsilon_t}{k_t} - C_2 s_L \frac{\Sigma}{\langle Y_R \rangle} \right\} \Sigma, \tag{45}$$

where D_t is a turbulent diffusivity; k_t is the turbulent kinetic energy and ϵ_t its rate of dissipation, both measured in the unburnt gas; C_1 and C_2 are model constants of order one. Equation (45) is based on the exact evolution equation given in (13). The first term on the right-hand side of (45) describes the transport of Σ by turbulent fluctuations and is obtained using a standard gradient flux approximation. The transport of Σ by flame propagation is considered negligible compared to the turbulent transport. The second term on the right-hand side of (45) describes the effects of flame stretch and has two components. The first component is a production term that accounts for straining due to the turbulent motions. This term corresponds to $\langle a_T \rangle_S$ in (13). The second component is a destruction term that accounts for the smoothing of the flame surface by flame propagation effects. This term corresponds to $2\langle w k_m \rangle_S$ in (13). Note that CFM does not explicitly represent the strain rate due to the mean flow field, $\langle A_T \rangle_S$. Thus, the basic closure assumptions used in CFM may be summarized as follows:

$$-\langle \boldsymbol{u}'' \rangle_S \Sigma = D_t \nabla \Sigma, \tag{46}$$

$$\langle a_T \rangle_S = C_1 \epsilon_t / k_t, \tag{47}$$

$$2\langle w k_m \rangle_S = -C_2 s_L \Sigma / \langle Y_R \rangle. \tag{48}$$

In (47), the mean strain rate is assumed to scale with the integral timescale of the turbulence. This choice is not unique and various estimates of $\langle a_T \rangle_S$ may be found in the literature. For instance, a more elaborate model where $\langle a_T \rangle_S$ is made a function of u'/s_L and l/l_F, and thereby includes some effects due to the chemistry, was recently proposed by Meneveau & Poinsot (1991). The propagation term is more difficult to

model. In (48), this term is modelled as a destruction term, an idea that is shared by all current formulations of the Σ-equation (Darabiha *et al.* 1987; Pope & Cheng 1988; Maistret *et al.* 1989; Candel *et al.* 1990; Cant *et al.* 1990).

The validity of any of these closure assumptions may be examined using the DNS database. We are particularly interested in the propagation term since, unlike turbulent diffusion and hydrodynamic straining which occur in other problems, this term describes physical processes that are unique features of premixed flames. Also, information on the combination of propagation and curvature is scarce and the exact significance of this combination is not well understood. In fact, the modelling of the propagation term in (48) is based as much on mathematical convenience as it is on physical insight. It appears as the most questionable closure assumption used in current formulations of the Σ-equation.

Figure 15(*a*) presents a comparison between the spatial variations of flame stretch as obtained from the simulations and the predictions by CFM based on (47) and (48). The comparison is performed at $t/\tau_0 \approx 4.3$, for $Le = 0.8$. We use for the model constants $C_1 = C_2 = 1$. Some aspects of this comparison are very encouraging. To its credit, the model is able to reproduce qualitatively the spatial structure of the balance between production and dissipation of Σ, going from production at the front of the turbulent flame to dissipation at the back. Several problems remain however.

One basic problem is that the propagation term in (48) is described as being always negative. This simplified description is certainly not valid, as shown in figure 14 where $2\langle wk_m\rangle_S$ is seen to change sign within the turbulent flame brush. It is also inconsistent with the underlying physics. Indeed, while negative values of the propagation speed, w, are possible in highly stretched flames, they remain rather unlikely and the sign of wk_m is primarily determined by the sign of the flame curvature, k_m. Since most flamelets at the leading edge of the turbulent flame are positively curved, the propagation term, $2\langle wk_m\rangle_S$, is positive in that region and contributes to flame surface production. In the simulations, this contribution is always significant and cannot be neglected, particularly for the $Le = 0.3$ and 0.8 unstable flames. In (48), failing to account for this dual nature of the propagation term, destruction at the back of the flame and production at the front, is likely to result in a model that is too dissipative.

Furthermore, it is found that the $\Sigma/\langle Y_R\rangle$ dependence of the destruction term in (48) leads to numerical difficulties on the burnt side of the flame, where both Σ and $\langle Y_R\rangle$ approach zero. In the simulations, $\langle Y_R\rangle$ goes to zero faster than Σ as $\langle c\rangle \to 1$, and the ratio $\Sigma/\langle Y_R\rangle$ is not well-behaved. As a result, CFM strongly overestimates the dissipation of flame surface area, locally near $\langle c\rangle = 1$, as well as globally when quantities are space-averaged. For instance, at time $t/\tau_0 \approx 4.3$, CFM predicts a negative total flame stretch, $\hat{\kappa} = -1.5$, in disagreement with the positive values reported in §4.2.2. In plain words, CFM predicts flame contraction when flame growth is observed.

It also appears that the modelling in (48) is incomplete. One remarkable result from the simulations is the large effect of the Lewis number on the overall production of flame surface area. This result is consistent with a growing body of evidence that shows persistence of thermo-diffusive effects in turbulent flames, even at high Reynolds numbers (Abdel-Gayed *et al.* 1984; Wu *et al.* 1990; see also Kuznetsov & Sabel'nikov 1990, chap. 6). CFM, however, as seen in (45), does not depend on the flame physical properties and therefore cannot account for changes in the Lewis number. The absence of thermo-diffusive effects in CFM, like in all flamelet models, is an open problem that remains to be addressed. We believe that the present analysis sets the basis for future studies of these effects, and others, and demonstrates the potential of DNS methods

that can be used to estimate the constituent parts of turbulent combustion models and thereby evaluate directly their underlying assumptions.

6. Conclusions

Direct simulations of premixed flames in isotropic turbulent flow are used in this paper to examine the flamelet description of the mean reaction rate with emphasis on the flame surface wrinkling. In the flamelet theory, the wrinkling is described by the flame surface density, Σ. The mean reaction rate is given by the product of the flame surface density, Σ, and the flamelet speed, $\langle S_C \rangle_S$.

The relationship between flame surface densities and mean reaction rates is studied for different Lewis numbers, $Le = 0.3$, 0.8, 1.0 and 1.2. The Lewis number is used as a control parameter to modify the strength and nature of the flame–flow coupling. For flames with Lewis numbers close to unity, $0.8 \leqslant Le \leqslant 1.2$, the departures of the flamelet speed from the one-dimensional laminar consumption rate average out; to first order the flame surface density is the single key quantity that determines the mean reaction rate. In contrast, for $Le = 0.3$, the effect of the turbulence on the flame surface area is coupled with a significant increase in the mean flame intensity, and both the flame surface density and the flamelet speed need to be modelled to determine the mean reaction rate.

For $Le = 1.0$ or 1.2, the combustion process is stable and the flame wrinkling is primarily controlled by the turbulent motions, but for lower Lewis numbers the combustion becomes highly unstable and the flame surface keeps increasing in time. The growth is nearly linear for $Le = 0.8$, and exponential for $Le = 0.3$.

A detailed analysis of the rate of change of flame surface densities is performed, based on the exact Σ-equation, in which basic physical mechanisms like transport by the turbulent flow field, transport by flame propagation, production or destruction by flame stretch, are described explicitly. A new DNS-based methodology is developed to estimate the different terms appearing in the Σ-equation. Using this methodology, the flame surface density and the flame stretch are resolved spatially across the turbulent flame brush. In the simulations, the two components of stretch, hydrodynamic strain rate and flame propagation effects, have the same order of magnitude. On the unburnt side of the reaction zone, these two components are both positive and the net effect corresponds to production of flame surface area. On the other hand, on the burnt side, the two components have opposite signs, and the overall balance is negative and corresponds to flame surface dissipation. Thus, contrary to the intuitive idea that flame propagation effects merely counteract the wrinkling due to the turbulence, the role of flame propagation is not constant across the reaction zone and switches from flame surface production at the front to flame surface dissipation at the back.

Additional results show that while a transition in the turbulent flame structure, as characterized by the flamelet speed, $\langle S_C \rangle_S$, occurs at $Le = 1$, a similar transition for the mean propagation speed, $\langle w \rangle_S$, does not occur until the Lewis number is decreased to a lower critical value, $Le_c < 1$. The present results show that $0.3 < Le_c < 0.8$, so that, in the $Le = 0.8$ case, the flame response is found to be paradoxical: the leading edge of the turbulent flame burns faster but propagates more slowly than the rear edge of the flame, which burns more slowly but propagates faster into the reactants. While Le_c is known to depend on the flame properties, like for instance the amount of heat release, one remaining question is whether Le_c is a function of the turbulence itself.

Direct comparisons with flamelet models are also performed. The empirical assumption in the Bray–Moss–Libby model that the flame surface density is

proportional to the flamelet crossing frequency is found to be valid. This result is the current basis for experimental measurements of flame surface densities. Unfortunately, large discrepancies are obtained when comparing the numerical results with the Bray–Moss–Libby description of the flamelet crossing frequency. This description does not account explicitly for the competing effects of hydrodynamic straining and flame propagation, which directly control the changes in flame surface area, and is therefore not well-suited to address problems where the balance between these effects is changing rapidly.

In comparison, the coherent flame model of Marble & Broadwell is based on the Σ-equation and incorporates explicitly the important physical mechanisms that determine the rate of change of flame surface area. Closure is thereby achieved at a more fundamental level. The spatial variations in the balance between production and destruction of flame surface area are correctly described by the model. However, the modelling of the combined effects of flame curvature and flame propagation needs further improvement. Also, the model, like most current flamelet models, is unable to reproduce thermo-diffusive effects which are found to be very important in the present simulations.

This research was performed in part during the second author's visit as a participant in the 1992 summer program of the Stanford University/NASA Ames Center for Turbulence Research (CTR). The authors acknowledge the fruitful interaction with other members of the combustion group during the summer program. In particular, we thank Dr F. Gao from CTR for his many insights into the diagnostics developed in this study. We also thank Professor S. B. Pope, Professor F. A. Williams, and Dr V. R. Kuznetsov for helpful comments and suggestions.

REFERENCES

ABDEL-GAYED, R. G., BRADLEY, D., HAMID, M. N. & LAWES, M. 1984 Lewis number effects on turbulent burning velocity. In *Twentieth Symp. (Intl) on Combustion*, pp. 505–512. The Combustion Institute.

ALDREDGE, R. C. & WILLIAMS, F. A. 1991 Influence of wrinkled premixed-flame dynamics on large-scale, low-intensity turbulent flow. *J. Fluid Mech.* **228**, 487–511.

ASHURST, W. T., PETERS, N. & SMOOKE, M. D. 1987 Numerical simulation of turbulent flame structure with non-unity Lewis number. *Combust. Sci. Tech.* **53**, 339–375.

BORGHI, R. 1990 Turbulent premixed combustion: further discussion on the scales of the fluctuations. *Combust. Flame* **80**, 304–312.

BRAY, K. N. C. 1980 Turbulent flows with premixed reactants. In *Turbulent Reacting Flows* (ed. P. A. Libby & F. A. Williams). Topics in Applied Physics, vol. 44, pp. 115–183. Springer.

BRAY, K. N. C. 1990 Studies of the turbulent burning velocity. *Proc. R. Soc. Lond.* A **431**, 315–335.

BRAY, K. N. C., CHAMPION, M. & LIBBY, P. A. 1989 The interaction between turbulence and chemistry in premixed turbulent flames. In *Turbulent Reactive Flows* (ed. R. Borghi & S. N. B. Murthy). Lecture Notes in Engineering, vol. 40, pp. 541–563. Springer.

BRAY, K. N. C., LIBBY, P. A. & MOSS, J. B. 1984 Flamelet crossing frequencies and mean reaction rates in premixed turbulent combustion. *Combust. Sci. Tech.* **41**, 143–172.

CANDEL, S. M. & POINSOT, T. 1990 Flame stretch and the balance equation for the flame surface area. *Combust. Sci. Tech.* **70**, 1–15.

CANDEL, S. M., VEYNANTE, D., LACAS, F., MAISTRET, E., DARABIHA, N. & POINSOT, T. 1990 Coherent flame model: applications and recent extensions. In *Recent Advances in Combustion Modelling* (ed. B. Larrouturou). World Scientific.

CANT, R. S., POPE, S. B. & BRAY, K. N. C. 1990 Modelling of flamelet surface-to-volume ratio in turbulent premixed combustion. In *Twenty-Third Symp. (Intl) on Combustion*, pp. 809–815. The Combustion Institute.

CHENG, R. K., SHEPHERD, I. G. & TALBOT, L. 1988 Reaction rates in premixed turbulent flames and their relevance to the turbulent burning speed. In *Twenty-Second Symp. (Intl) on Combustion*, pp. 771–780. The Combustion Institute.

CHEW, T. C., BRAY, K. N. C. & BRITTER, R. E. 1990 Spatially resolved flamelet statistics for reaction rate modeling. *Combust. Flame* **80**, 65–82.

CLAVIN, P. 1985 Dynamic behavior of premixed flame fronts in laminar and turbulent flows. *Prog. Energy Combust. Sci.* **11**, 1–59.

CLAVIN, P. & GARCIA, P. 1983 The influence of temperature dependence of diffusivities on the dynamics of flame fronts. *J. Méc.* **2**, 245–263.

CLAVIN, P. & WILLIAMS, F. A. 1982 Effects of molecular diffusion and of thermal expansion on the structure and dynamics of premixed flames in turbulent flows of large scale and low intensity. *J. Fluid Mech.* **216**, 251–282.

DARABIHA, N., GIOVANGIGLI, V., TROUVÉ, A., CANDEL, S. M. & ESPOSITO, E. 1987 Coherent flame description of turbulent premixed ducted flames. In *Turbulent Reactive Flows* (ed. R. Borghi & S. N. B. Murthy). Lecture Notes in Engineering, vol. 40, pp. 591–637. Springer.

DRISCOLL, J. F. & GULATI, A. 1988 Measurement of various terms in turbulent kinetic energy balance within a flame and comparison with theory. *Combust. Flame* **72**, 131–152.

DRISCOLL, J. F., SUTKUS, D. J., ROBERTS, W. L., POST, M. E. & GOSS, L. P. 1993 The strain exerted by a vortex on a flame – Determined from velocity field images. *31st Aerospace Sciences Meeting, Reno NV, Paper* 0362. AIAA.

DUCLOS, J. M., VEYNANTE, D. & POINSOT, T. 1993 A comparison of flamelet models for premixed turbulent combustion. *Combust. Flame* **95**, 101–117.

GOIX, P. J. & SHEPHERD, I. G. 1992 Lewis number effects on turbulent premixed flame structure. *Fall Meeting of the Western States Section.* The Combustion Institute.

HAWORTH, D. C. & POINSOT, T. 1992 Numerical simulations of Lewis number effects in turbulent premixed flames. *J. Fluid Mech.* **244**, 405–436.

KERSTEIN, A. R., ASHURST, W. T. & WILLIAMS, F. A. 1988 Field equation and interface propagation in an unsteady homogeneous flow field. *Phys. Rev.* A **37**, 2728–2731.

KUZNETSOV, V. R. & SABEL'NIKOV, V. A. 1990 *Turbulence and Combustion.* Hemisphere.

LAW, C. K. 1988 Dynamics of stretched flames. In *Twenty-Second Symp. (Intl) on Combustion*, pp. 1381–1402. The Combustion Institute.

LEE, T. W., NORTH, G. L. & SANTAVICCA, D. A. 1992 Curvature and orientation statistics of turbulent premixed flame fronts. *Combust. Sci. Tech.* **84**, 121–132.

LELE, S. K. 1992 Compact finite difference schemes with spectral-like resolution. *J. Comput. Phys.* **103**, 16–42.

LIBBY, P. & WILLIAMS, F. A. 1983 Strained premixed laminar flames under nonadiabatic conditions. *Combust. Sci. Tech.* **31**, 1–42.

MAISTRET, E., DARABIHA, N., POINSOT, T., VEYNANTE, D., LACAS, F., CANDEL, S. M. & ESPOSITO, E. 1989 Recent developments in the coherent flamelet description of turbulent combustion. In *Proc. 3rd Intl SIAM Conf. on Numerical Combustion.*

MANTEL, T. & BORGHI, R. 1994 A new model of premixed wrinkled flame propagation based on a scalar dissipation equation. *Combust. Flame* **96**, 443–457.

MARBLE, F. E. & BROADWELL, J. E. 1977 The coherent flame model for turbulent chemical reactions. *Project Squid Tech. Rep.* TRW-9-PU.

MATALON, M. 1983 On flame stretch. *Combust. Sci. Tech.* **31**, 169–181.

MATALON, M. & MATKOWSKY, B. J. 1982 Flames are gasdynamic discontinuities. *J. Fluid Mech.* **124**, 239–259.

MENEVEAU, C. & POINSOT, T. 1991 Stretching and quenching of flamelets in premixed turbulent combustion. *Combust. Flame* **86**, 311–332.

PELCÉ, P. & CLAVIN, P. 1982 Influence of hydrodynamics and diffusion upon the stability limits of laminar premixed flames. *J. Fluid Mech.* **124**, 219–237.

PETERS, N. 1986 Laminar flamelet concepts in turbulent combustion. In *Twenty-First Symp. (Intl) on Combustion*, pp. 1231–1250. The Combustion Institute.

POINSOT, T. & LELE, S. K. 1992 Boundary conditions for direct simulations of compressible viscous flows. *J. Comput. Phys.* **101**, 104–129.

POINSOT, T., ECHEKKI, T. & MUNGAL, M. G. 1992 A study of the laminar flame tip and implications for premixed turbulent combustion. *Combust. Sci. Tech.* **81**, 45–73.

POINSOT, T., VEYNANTE, D. & CANDEL, S. M. 1991 Quenching processes and premixed turbulent combustion diagrams. *J. Fluid Mech.* **228**, 561–605.

POPE, S. B. 1988 Evolution of surfaces in turbulence. *Intl J. Engng Sci.* **26**, 445–469.

POPE, S. B. 1990 Computations of turbulent combustion: progress and challenges. In *Twenty-Third Symp. (Intl) on Combustion*, pp. 591–612. The Combustion Institute.

POPE, S. B. & CHENG, W. K. 1988 The stochastic flamelet model of turbulent premixed combustion. In *Twenty-Second Symp. (Intl) on Combustion*, pp. 781–789. The Combustion Institute.

ROBERTS, W. L., DRISCOLL, J. F., DRAKE, M. C. & GOSS, L. P. 1993 Images of the quenching of a flame by a vortex: to quantify regimes of turbulent combustion. *Combust. Flame* **94**, 58–69.

RUTLAND, C. J. & TROUVÉ, A. 1993 Direct simulations of premixed turbulent flames with non-unit Lewis numbers *Combust. Flame* **94**, 41–57.

WILLIAMS, F. A. 1985 *Combustion Theory*, 2nd edn. Benjamin Cummings.

WRAY, A. A. 1990 Minimal storage time-advancement schemes for spectral methods. *Tech. Rep. NASA Ames Research Center*, M.S. 202 A-1.

WU, M. S., KWON, S., DRISCOLL, J. F. & FAETH, G. M. 1990 Turbulent premixed hydrogen/air flames at high reynolds numbers. *Combust. Sci. Tech.* **73**, 327–350.